# Discovery of cephalotaxinone enzymes reveals a whole plant model for homoharringtonine biosynthesis

Yaereen Dho,[1] Kevin Smith,[2] & Elizabeth S. Sattely[2,3]*

[1]Department of Chemistry, Stanford University, Stanford, CA 94305

[2]Department of Chemical Engineering, Stanford University, Stanford, CA 94305

[3]HHMI, Stanford University, Stanford, CA 94305

*corresponding author

## ABSTRACT

Plants produce diverse molecules that inhibit protein translation. A lead example is homoharringtonine (HHT), a key tool for ribosomal profiling and an FDA-approved treatment for chronic myeloid leukemia. HHT is commercially produced through semi-synthesis from the alkaloid core cephalotaxine (CET) extracted from endangered *Cephalotaxus* species. Despite its significance, the CET/HHT biosynthetic pathway remains unresolved. Here, we use paired untargeted metabolomics (stable-isotope precursor feeding) and transcriptomics to elucidate a near-complete biosynthesis to CET without prior knowledge of intermediates and biosynthetic genes. We show that while the CET core is biosynthesized only in growing root tips, CET and HHT accumulate throughout the plant. We discovered seven pathway intermediates and six novel enzymes that produce cephalotaxinone, the likely direct precursor of CET. Included are non-canonical cytochrome P450s, an atypical short-chain dehydrogenase, and a 2-oxoglutarate-dependent dioxygenase that together result in carbon excision and CET/HHT pentacyclic backbone formation. This study establishes a metabolic route to the HHT core scaffold and suggests a whole-plant coordination model in *Cephalotaxus*, where cephalotaxinone is produced in root tips and distributed throughout the plant for subsequent elaboration to HHT.

## MAIN TEXT

*Cephalotaxus* (plum yew) is a slow-growing coniferous tree from the *Cephalotaxaceae* family that produces over 70 structurally diverse *Cephalotaxus* alkaloids with the most prominent being cephalotaxine (CET)—the core structure of *Cephalotaxus* alkaloids[1-3]. Although no unique bioactivity for CET itself has been reported, its ester derivatives—such as harringtonine, isoharringtonine, deoxyharringtonine, and homoharringtonine (HHT)—have demonstrated potent antileukemic activity *in vivo*, each significantly inhibiting P388 lymphoid leukemia in mice at doses as low as 1 mg/kg[2,4-6]. HHT, in particular, exhibited nanomolar inhibitory activity against myeloid and lymphocytic leukemia cell lines[7] and was approved by the U.S. Food and Drug Administration (FDA) in 2012 for the treatment of chronic myeloid leukemia (CML)[8,9], especially in patients resistant to tyrosine kinase inhibitors (comprising 30% of CML cases)[10]. Also known as omacetaxine mepesuccinate (Synribo®), the HHT drug acts as a protein translation inhibitor by binding to the A-site of the eukaryotic large ribosomal subunit, preventing the initial elongation step in protein synthesis[11-14]. The specificity of harringtonine alkaloids has also made it a critical research tool in ribosomal profiling[15].

Despite its biomedical value, HHT remains difficult to access. Natural levels of HHT in *Cephalotaxus* species are extremely low (~0.06-3.2 mg/g dry weight)[16,17], and its current commercial production primarily relies on a semi-synthetic route involving the extraction of CET from *Cephalotaxus* needles, followed by chemical esterification with a synthetic side chain[1,18-20]. While total syntheses of CET and HHT have been reported[18,21,22], these approaches are limited by multi-step procedures and low

yields, making them commercially less favorable. Furthermore, *Cephalotaxus* species have been classified as endangered due to extensive harvesting, inherently slow growth rate, and long seed development time[1,2,23]. Since late 2024, although still listed in FDA-approved drug, HHT has been discontinued in the U.S. in part due to manufacturing limitations[24,25], underscoring the need for alternative production platforms. Metabolic engineering of *Cephalotaxus* alkaloid biosynthesis into tractable heterologous hosts could provide a sustainable, scalable production of CET and HHT; however, the development of such solutions has been impeded by a fundamental lack of knowledge of their biosynthetic pathways. Furthermore, knowledge of biosynthetic genes would enable studies to determine the specific biological role of these alkaloids in the producing species.

Early radioisotope labeling studies in actively growing *Cephalotaxus harringtonia* demonstrated that CET is derived from the amino acids tyrosine[26,27] and phenylalanine[27,28] (Figure 1). Based on these findings—and the minor presence of homoerythrina-type alkaloids in *Cephalotaxus* species—it was hypothesized that a phenethylisoquinoline scaffold is an intermediate of CET biosynthesis, formed from tyrosine and phenylalanine via a pathway analogous to those described for *Colchicum* and *Schelhammera* alkaloids[2,26-28]. However, the failure of cinnamic acid to incorporate into CET has questioned the validity of this hypothesis[2,27]. More recently, a phenethylisoquinoline scaffold (**1**) was reported in *C. hainanensis*, along with upstream biosynthetic enzymes capable of converting tyrosine and phenylalanine into **1**[29], resembling the early steps in colchicine biosynthesis[30]. These findings support a biosynthetic pathway model that hinges on this Pictet-Spengler metabolite, but to date, there is no direct evidence that this compound **1** is a precursor to CET or HHT alkaloids (**Fig. 1**) and no additional pathway intermediates have been identified. Moreover, CET and HHT are found distributed throughout the plant body, and thus a site of active biosynthesis has remained elusive[2,16]. Collectively, these gaps have made elucidating the biosynthetic pathways of *Cephalotaxus* alkaloids particularly challenging.

Here, we address these long-standing challenges by generating paired metabolomic (via isotope-labeled precursor feeding) and transcriptomic datasets across diverse tissues of *C. harringtonia* harvested during its actively growing season. This integrated approach revealed a site of active biosynthesis of CET, uncovered previously unknown key intermediates, and ultimately enabled the discovery of a set of highly co-expressed biosynthetic enzymes responsible for biosynthesis of the CET core.

## RESULTS

### Labeling studies identify growing root tips as a site of active biosynthesis of CET and specific phenethylisoquinolines as intermediates in the pathway

In studying biosynthetic pathways of metabolites of interest in non-model plants like *Cephalotaxus harringtonia*, where genomic resources and genetic manipulation tools are limited, transcriptomics with co-expression analyses has often been used when the spatial, temporal, or condition-specific production of the compounds is known[31-34]. However, sequencing a plant transcriptome without prior knowledge of when and where the pathway is expressed may not capture relevant biosynthetic genes. Moreover, knowledge of the correct biosynthetic intermediates is also crucial for the discovery of biosynthetic genes. In our prior work using a $D_2O$ labeling study, we proposed that HHT is actively biosynthesized in new growth needles of *Cephalotaxus*[35]. However, it was unclear whether the entire pathway or only a portion (i.e. the final steps) is active in these tissues. Given that our efforts to identify biosynthetic genes expressed in these tissues were unsuccessful[36], we considered whether parts of the pathway were expressed in other plant tissues. Thus, we first attempted to identify a site of active biosynthesis for the alkaloid core, CET, specifically and elucidate potential intermediates in the pathway with stable-isotope precursor feeding experiment across different tissues of *C. harringtonia*.

To collect various tissues of *C. harringtonia*, we harvested plant tissues (young inner needles—YIN, young outer needles—YON, old needles—ON, young stem—YSt, old stem—OSt, and root tips—Rt) when the plant appears to be actively growing—this was typically spring[16,37,38] (**Fig. 2a**). We then first compared natural accumulation of CET and HHT in different tissues using liquid chromatography-mass spectrometry (LC-MS). Both CET (**Fig. 2b**, left) and HHT (**Fig. 2b**, right) were detected at high levels in all different tissues collected in May 2022, with lowest in YSt. CET was about 50- to 200-fold higher in amount than HHT throughout the plant (**Supplementary Fig. 1a**). Tissue samples collected in May 2023 were also analyzed and compared (**Supplementary Fig. 1b** and **1c**). In both sample sets, both CET and HHT are generally abundant in all tissues with no consistent pattern of accumulation.

To determine whether CET and HHT are actively made in all different tissues, as detected, or synthesized in a specific tissue and transported throughout the plant, we next conducted a stable isotope precursor feeding experiment with samples from various parts of an actively growing plant. Sectioned tissues of *C. harringtonia* were incubated in a solution of dopamine-$D_4$ (deuterium-labeled alkyl groups), a predicted early intermediate in CET biosynthesis based on the prior isotope labeling study that showed tyrosine serving as an upstream precursor[26,27] and on the hypothesis that CET biosynthesis involves a phenethylisoquinoline scaffold[2,26,29]. Interestingly, enrichment of CET-$D_4$ ($[M_0 + H_4 + H]^+$ = *m/z* 320.1794) was observed only in the root tips (up to length of approximately 5-8 cm)—Rt, and not in other tissues (**Fig. 2c** and **Supplementary Fig. 2**). These results support a model where CET biosynthesis from dopamine occurs at the root tips of an actively growing plant, contrasting with the widespread accumulation pattern of CET, and that dopamine serves as a key pathway precursor.

We then performed an untargeted metabolite analysis (XCMS) comparing dopamine-$D_4$-fed root tips with water-fed controls to search for pathway intermediates. A ranking using increasing fold change in abundance between the two conditions (fold change > 3.5 and $P < 0.2$), with *m/z* in between 200 and 600, revealed several deuterium ($D_4$) labeled metabolites that may serve as potential intermediates in CET biosynthesis. Notably, these mass features each have an *m/z* close to CET and a large fold-change relative to others in the list of 148 unique mass features found (**Fig. 2d** and Supplementary **Fig. 1d**). We searched for both the deuterated and unlabeled isotopes of these molecules using extracted ion chromatograms (EICs) from both dopamine-$D_4$ and water treated root tips and found that while the unlabeled isotopes were present in both sample sets, the deuterated isotopes accumulated only in dopamine-$D_4$-treated samples. These results indicate that these molecules not only arise from dopamine-$D_4$ but also are true metabolites of *C. harringtonia*. Interestingly, the first two mass signatures in the ranked list were found to correspond to specific phenethylisoquinoline scaffolds (**2**-$D_4$ and **3**-$D_4$) when compared to authentic synthesized standards (**Supplementary Fig. 3**). Unlike CET that was found throughout the plant body, **2** and **3** accumulated only in root tips (**Supplementary Fig. 1e-f**). Nonetheless, their $D_4$-enrichment (**2**-$D_4$ and **3**-$D_4$) from dopamine-$D_4$ feeding showed a similar pattern to that of CET-$D_4$, which occurs exclusively in growing root tips and not in other tissues (**Supplementary Fig. 1g-h**). These results suggested that **2** and **3** could be intermediates of CET biosynthesis and that they could represent sequential metabolism since they differ only by an O-methylation. Meanwhile, untargeted analyses also identified CET-$D_4$. Its relatively low fold change (3.8) compared to earlier potential intermediates could be attributed to its position further downstream in the pathway. Three additional mass signatures with large fold change and interesting *m/z* that are close to that of CET (**Fig. 2d**, red dots) were subsequently also found to be true intermediates of CET biosynthetic pathway (see **Fig. 4** and **Extended Data Figs. 9-10**), suggesting that feeding of early precursor (dopamine-$D_4$ in this case) combined with untargeted analyses using LC-MS effectively revealed intermediates of interest.

To determine whether **2** is an intermediate of CET biosynthesis, different tissues of actively growing *C. harringtonia* were sectioned and soaked in a solution of **2**-$D_4$ and analyzed with LC-MS in a manner similar to the dopamine-$D_4$ feeding study. Relative isotope enrichment of CET-$D_4$ in **2**-$D_4$ feeding compared to water treatment in six different tissues further supports the growing root tips as a site of active biosynthesis of CET and that **2**-$D_4$ serves as a pathway intermediate (**Fig. 2e**). Furthermore, unlike

138 when dopamine-$D_4$ was fed, **3**-$D_4$ was observed in all different tissues when treated with **2**-$D_4$.
139 Nevertheless, O-methylation of **2**-$D_4$ to **3**-$D_4$ predominantly occurred in the growing root tips compared to
140 other tissues (**Fig. 2f** and **Supplementary Fig. 1i**), following a similar pattern of high **3**-$D_4$ enrichment in
141 root tips from dopamine-$D_4$ feeding (**Supplementary Fig. 1h**).

142 Since both dopamine and **2** are incorporated into **3** and appear to be involved in CET biosynthesis
143 in root tips, we next sought to determine whether **3** is a direct intermediate in the CET biosynthetic
144 pathway rather than a side-product or unrelated metabolite. Similar feed-in experiments and analyses
145 done with dopamine-$D_4$ and **2**-$D_4$ were conducted with **3**-$D_4$. Enrichment of CET-$D_4$ from **3**-$D_4$ feeding
146 occurred only in growing root tips and not in other tissues sampled (**Fig. 2g** and **Supplementary Fig. 1j**),
147 indicating that **3** serves as a true intermediate in CET biosynthesis and further supporting that a site of
148 active biosynthesis of CET is growing root tips and not other tissues. Furthermore, our identification of **2**
149 and **3** reveals direct evidence for CET biosynthetic intermediates beyond the tyrosine and phenylalanine
150 precursors that had been identified in the 1970s[26-28] and provides experimental evidence for the long-
151 standing hypothesis that phenethylisoquinolines act as intermediates in CET biosynthesis[2,26].

152 Because **2** and **3** were both found to be intermediates of CET, and phenethylisoquinolines—
153 especially compound **1**—have long been hypothesized to be intermediates of CET[2,26], we also searched
154 for other possible phenethylisoquinolines such as **1**, **11**, **12**, and **13** to examine their biological relevance,
155 and whether they could serve as potential intermediates in the CET pathway (**Supplementary Figs. 4-5**
156 and **Supplementary Table 1**). Although natural accumulation of **1**[29] and **11** were observed in root tips of
157 *C. harringtonia*, we did not detect enrichment of **1**-$D_4$ nor **11**-$D_4$ following feeding of dopamine-$D_4$
158 (**Supplementary Fig. 4**). Moreover, neither **12** nor **13** were detected anywhere in any tissues of *C.*
159 *harringtonia* sampled (**Supplementary Fig. 5**). We also did not detect deuterium enrichment of **12** and
160 **13** (**12**-$D_4$ and **13**-$D_4$) from feeding dopamine-$D_4$. Feeding of **1**-$D_4$ and **12**-$D_4$ in different tissues sampled
161 from *C. harringtonia* also did not result in enrichment of CET-$D_4$ (**Supplementary Figs. 4-5**). These
162 findings collectively suggested that CET is derived from **2**, which is formed through a Pictet-Spengler-
163 like condensation of dopamine and 3-(4-hydroxy-3-methoxyphenyl)propanal (**Fig. 2h** and
164 **Supplementary Table 1**). Compounds **1** and **11** are likely not on pathway to CET but represent
165 additional alkaloids that accumulate in *Cephalotaxus* roots but were not actively made during the time of
166 sampling.

167 Additionally, unlike CET, no enrichment of deuterated HHT (HHT-$D_4$) was detected in any of the
168 sectioned tissues of *C. harringtonia* fed with dopamine-$D_4$, **2**-$D_4$, or **3**-$D_4$. This result may be interpreted
169 in two ways: i) the feed-in assay failed to capture HHT biosynthesis despite root tips being the sole site of
170 HHT production, or ii) the alkaloid core of HHT gets made only in roots and is transported to other parts
171 of the plant, where side-chain biosynthesis and its attachment occur to produce HHT. The widespread
172 availability of both CET and HHT in all different tissues likely support the latter model.

173 Collectively, the stable-isotope labeled precursor feeding studies with various tissues sectioned
174 from an actively growing *C. harringtonia* revealed that the root tips are the primary site of CET alkaloid
175 core biosynthesis, which does not align with the widespread accumulation pattern of CET and HHT
176 observed throughout the plant. The biosynthetic pathway begins with tyrosine[26,27] and phenylalanine[27,28]
177 and proceeds through the intermediates dopamine, **2**, and **3**. Compound **3** likely undergoes oxidative
178 coupling to form compound **6** (a proposed intermediate with a mass signature identified via XCMS
179 analyses; **Fig. 2d**), followed by a series of oxidations, including carbon excision, and reduction to
180 ultimately produce CET (**Fig. 2h**). Our data suggest that the alkaloid core of HHT is biosynthesized and
181 subsequently transported from root tips and distributed throughout the plant, where side-chains are
182 attached when needed to produce the toxic ester-derivatives such as HHT[1,2,4]. The availability of
183 downstream intermediates (**2** and **3**) exclusive to root tips further supports our model. Having identified **2**
184 and **3** as intermediates in the pathway, we next sought to identify a candidate gene in biosynthesis that
185 could be used as a bait gene to shortlist candidate CET biosynthetic enzymes.

186

187 **Paired transcriptomics and metabolomics analysis identifies *Ch*OMT-1 as the biosynthetic gene and**
188 **reveals co-expressed candidate genes involved in CET biosynthesis**

189 Transcriptomics with co-expression analyses has often been used in elucidating plant biosynthetic
190 pathways when spatial, temporal, or condition-specific production of a compound of interest is known[31-
191 34,39]. With the knowledge that a site of active CET biosynthesis is specific to root tips, we sought to use
192 transcriptional analyses to identify CET biosynthetic enzymes. To do so, we first aimed to obtain a
193 transcriptome of *C. harringtonia* that fully captures CET biosynthetic genes by generating our own *in-*
194 *house* transcriptome paired with stable-isotope labeling studies on diverse tissues of actively growing *C.*
195 *harringtonia*, harvested in May 2023. Each tissue sample was divided for parallel profiling (one for
196 metabolomics and the other for transcriptomics), ensuring that the biosynthetically active root tip tissues
197 were analyzed using RNA-seq. We also utilized PacBio Iso-Seq to avoid technical limitations of de novo
198 transcriptome assembly, such as misassembled or fragmented contigs[39,40], and obtain an accurate, full-
199 length transcriptome that could be used as a reference for short-read RNA-seq (29,163 transcripts after
200 processing). Illumina sequencing from multiple various plant tissues (a total of 36 biosynthetic and non-
201 biosynthetic samples) was then used to quantify relative gene expression.

202 Using these paired metabolomic and transcriptomic datasets across diverse tissues of *C.*
203 *harringtonia*, we sought to identify an initial enzyme in CET biosynthetic pathway that could be used as a
204 bait gene for co-expression analyses to discover CET biosynthetic enzymes. With the knowledge that O-
205 methylation of **2** to **3** is involved in CET biosynthesis in root tips, we proposed that the enzyme
206 responsible for this transformation of **2** to **3** would be a good first candidate to be used as the bait gene.
207 Because O-methylation of **2** to **3** mainly occurs in the root tips of the plant and *S*-adenosylmethionine-
208 dependent methyltransferase is a family of enzymes known for performing O-methylation[30,41], we focused
209 on transcripts that had expression in roots and their Pfam annotated as methyltransferase. We then
210 prioritized our candidate gene list by conducting a Pearson's correlation ($r > 0.85$) between transcript
211 expression levels and **3**-$D_4$ enrichment across all 15 tissues fed with **2**-$D_4$. These analyses together
212 resulted in a shortlist of 18 methyltransferase-annotated transcripts, whose expression strongly correlated
213 with *in vivo* metabolic conversion of **2**-$D_4$ to **3**-$D_4$ (**Fig. 3a** and **Supplementary Fig. 6**).

214 A batch of 5 out of the 18 that were initially cloned from *C. harringtonia* cDNA was tested for
215 function using *Agrobacterium*-mediated transient expression in *N. benthamiana* leaves with direct co-
216 infiltration of **2** as a substrate[30,42]. LC-MS analysis of infiltrated leaf extracts revealed that one candidate
217 methyltransferase (YD-1-Rt_50321, highlighted in bold in **Fig. 3a**) consumed **2** and produced **3** (**Fig. 3b**
218 and **Supplementary Fig. 7**). This O-methyltransferase responsible for O-methylation of **2** to **3** was
219 referred to as *Ch*OMT-1.

220 *Ch*OMT-1 was then utilized as the bait gene to identify a set of strongly co-expressing CET
221 biosynthetic gene candidates from 29,163 unique transcripts. Initial Pearson correlation analysis across all
222 36 tissue samples using *Ch*OMT-1 as the query gene identified 316 highly co-expressed transcripts ($r >$
223 $0.98$). As many of these accumulate primarily in root tips and are not detected in other tissues, a second
224 round of correlation analysis ($r > 0.90$) was conducted using Rt samples alone, enabling prioritization of
225 41 top candidates (**Fig. 3c** and **Supplementary Fig. 8**). This top-ranking candidate list is rich in genes
226 that are generally associated with secondary metabolism such as cytochrome P450s (CYPs)[30,32,43],
227 Fe(II)/2-oxoglutarate-dependent dioxygenases (2OGDs)[39,44,45], and dehydrogenase/reductase enzymes[46,47],
228 suggesting that it contains CET biosynthetic enzymes responsible for oxidations and reductions that are
229 required to form CET from **3**. Furthermore, the list contains early CET biosynthetic genes that encode
230 enzymes, which have been previously shown to generate dopamine from tyrosine (*Ch*TyDC-1 and
231 *Ch*PPO-1)[29].

232

233 **Discovery and engineering of *Cephalotaxus* alkaloid biosynthesis**

234 With a shortlist of candidate CET biosynthetic genes from co-expression analysis (**Fig. 3c**) and
235 unique masses of the next top two potential intermediates (**6** and **5**) after **2** and **3** identified from
236 untargeted metabolite analysis (XCMS) of stable-isotope precursor feeding study (**Fig. 2d**), we next
237 sought to elucidate the downstream biosynthetic pathway of CET after **3**. To eventually produce CET, we
238 hypothesized that **3** would go through a series of oxidations such as oxidative coupling of two
239 methoxyphenols to form **6** and carbon excision from the lower six-membered ring C to form the five-
240 membered ring C' of CET (**Fig. 2h** and **Fig. 4b**).

241 We speculated that **3** first undergoes oxidative transformation: hydroxylation, oxidative coupling,
242 or both. All the oxidases (10 CYPs and 3 2OGDs)[32,45,48-50] in the shortlist of candidate genes (**Fig. 3c**)
243 were each cloned and tested by *Agrobacterium*-mediated transient transformation in *N. benthamiana* with
244 **3** co-infiltrated as a substrate. However, LC-MS analysis of leaf extracts revealed that none of the
245 candidates resulted in additional hydroxylation ($[M + H]^+$ = *m/z* 346.1649), oxidative coupling ($[M + H]^+$
246 = *m/z* 328.1543), or both ($[M + H]^+$ = *m/z* 344.1492) of **3**. However, one of the tested enzymes
247 (*Ch*CYP805A11) resulted in partial consumption of **3**. We therefore conducted untargeted metabolite
248 analysis (XCMS, see Methods) comparing *Ch*CYP805A11-expressed leaves to GFP-expressed leaves
249 (negative control), both co-infiltrated with **3**, to examine if any relevant unique mass with a significantly
250 increasing fold change ($\Delta > 5$) in abundance between the two conditions ($P < 0.1$) appeared (**Extended**
251 **Data Fig. 1**). XCMS analysis reported 27 unique masses, of which 7 are above the signal to noise
252 threshold and can be identified in the raw LC-MS data. These seven (**Extended Data Fig. 1d**, red dots)
253 all represent isotopologues or ions of a single compound ($[M + H]^+$ = *m/z* 348.1805, r.t. = 7.07 min) that
254 corresponds to a single hydroxylation and reduction of **3**. Based on the MS/MS analyses of both the
255 molecule and its four-deuterated form from **3**-$D_4$ feeding in root tips of *C. harringtonia* experiment, the
256 compound was assigned the structure of **4** (**Extended Data Fig. 1**). These results suggested that
257 *Ch*CYP805A11 catalyzes oxidative coupling of two methoxyphenols of **3** (rings A and C), forming **4'**
258 (**Fig. 4**). However, due to its unstable imine ring, **4'** likely undergoes imine hydrolysis to form **4''** that
259 contains a very reactive aldehyde moiety, which then gets reduced by a promiscuous reductase in *N.*
260 *benthamiana* to form **4** (**Extended Data Fig. 1h**). The instability of **4'** could explain why this molecule
261 was not detected in LC-MS but instead, a mass corresponding to a single hydroxylation and reduction of
262 **3** (**4**, $[M + H]^+$ = 348.1805 Da) was observed. This observation was consistent with metabolites observed
263 in the native plant *C. harringtonia*, indicating that the promiscuous reductase is not specifically present
264 only in *N. benthamiana* but also in other plants in general.

265 To form the fused bicyclic backbone of CET (rings B' and D), it has been speculated that a
266 precursor similar to **5**, formed through oxidative coupling of phenethylisoquinoline, undergoes an
267 intramolecular cyclization via nucleophilic attack by the nitrogen atom[2,51,52], indicating that the ring B'' of
268 **4'** needs to be preserved (**Fig. 4b**). We thus hypothesized that there exists a reductase in CET biosynthesis
269 for reducing the imine bond of **4'** to form the stable compound (**5**) and that **4** is not a direct intermediate
270 but a side-product of CET biosynthesis. To evaluate our hypothesis, all five
271 dehydrogenases/reductases[46,47,53,54] in the shortlist of candidate genes (**Fig. 3c**), including an atypical
272 short-chain dehydrogenase (SDR)—nitrogen metabolite repression regulator (NmrA)-like family
273 enzyme[55-59] (*Ch*NmrA-1) (sequence analyses of homologs, **Supplementary Fig. 9**), were each cloned and
274 co-expressed with *Ch*CYP805A11 in *N. benthamiana* leaves using *Agrobacterium*-mediated gene
275 delivery, with **3** co-infiltrated as a substrate. LC-MS analysis of the *Ch*NmrA-1 infiltrated leaf extracts
276 revealed partial reduction of **4** and production of a new peak ($[M + H]^+$ = *m/z* 330.1700, r.t. slightly left to
277 that of **3**) (**Extended Data Fig. 2**). This new peak corresponded to the compound with the fourth largest
278 fold-change in earlier XCMS analysis comparing dopamine-$D_4$-fed root tips with water-fed controls of *C.*
279 *harringtonia* (**Fig. 2d**), suggesting that it is likely to be an intermediate of CET biosynthesis. MS/MS
280 analyses of both the new molecule and its four-deuterated form were used to assign the structure as **5**
281 (**Extended Data Fig. 2**). Collectively, the results support our hypothesis that **3** goes through a

*Ch*CYP805A11 mediated oxidative coupling to form an unstable intermediate **4'**, which gets reduced by *Ch*NmrA-1 to produce **5**.

To further verify the functions of *Ch*CYP805A11 and *Ch*NmrA-1, *in vitro* assays with yeast microsomal protein fractions of *Ch*CYP805A11 and purified *Ch*NmrA-1 were conducted (**Extended Data Fig. 3**). Unlike in *N. benthamiana*, production of **4** was not detected in *in vitro* assays with purified yeast microsomes containing *Ch*CYP805A11 and incubated with **3**. Aside from trace amounts of **5**—potentially arising from non-enzymatic reduction in the presence of excess NADPH, we did not see any single new product based on untargeted metabolite analysis comparing purified yeast microsomes of *Ch*CYP805A11 to empty vector microsomes (negative control) in the absence of *Ch*NmrA-1, despite near-complete consumption of **3**. However, when both the microsomes of *Ch*CYP805A11 and purified *Ch*NmrA-1 were combined with **3** *in vitro*, production of **5** was observed by LC-MS. Moreover, treatment of *Ch*CYP805A11 microsomes incubated with **3** followed by $NaBD_3CN$ (an imine reducing agent)[60], in place of active *Ch*NmrA-1, resulted in formation of **5**-D (**Extended Data Fig. 3h-k**). These findings suggest that *Ch*CYP805A11 acts on **3**, producing an unstable intermediate, proposed to be **4'**, which can be reduced enzymatically by *Ch*NmrA-1 to form **5** (see **Supplementary Fig. 10** for proposed mechanism) or chemically by $NaBD_3CN$ to form **5**-D. Thus, the likely direct product of *Ch*CYP805A11 and the substrate for *Ch*NmrA-1 is **4'** rather than **4** (a reduced form of the aldehyde derived from hydrolysis of **4'**, proposed to form through promiscuous plant reductase).

As discussed earlier, we next speculated that **5** goes through an oxidative intramolecular cyclization via nucleophilic attack by the nitrogen atom to produce the fused bicyclic backbone of CET[2,51,52] (**Fig. 4b**). Therefore, the rest of 9 CYPs and 3 2OGDs in the shortlist of candidate genes (**Fig. 3c**) were each tested in combination with *Ch*CYP805A11 and *Ch*NmrA-1 in *N. benthamiana* leaves with co-infiltrating **3** as a substrate. Addition of *Ch*CYP805A12 resulted in consumption of **5** and production of a new peak, proposed to be **6** based on its MS/MS fragmentation pattern (**Extended Data Fig. 4**). This was the first intermediate identified containing a tertiary amine and a bicyclo[5.3.0]decane core (rings B' and D) that are crucial to the structural backbone of CET. Compound **6** also corresponded to the molecule with third largest fold-change in earlier XCMS analysis comparing dopamine-$D_4$-fed root tips with water-fed controls of *C. harringtonia* (**Fig. 2d**), indicating that LC-MS-based untargeted analyses of early precursor feeding studies in dissected tissues of a native plant could be used as an effective tool to identify biosynthetic intermediates.

To produce CET from **6**, a carbon excision from ring C and formation of methylenedioxy bridge in ring E are necessary (**Fig. 4b**). Because CYPs and 2OGDs have been known to catalyze such unusual oxidative transformations[39,48,49,61,62], the remaining 8 CYPs and 3 2OGDs in the shortlist of candidate genes (**Fig. 3c**) were again each tested in the transient expression system, producing **6**, and analyzed using LC-MS/MS. Interestingly, each *Ch*2OGD-1 and *Ch*CYP805A13 resulted in consumption of **6** and formation of different compounds, **7** (**Extended Data Fig. 5**) and **8** as well as **9** (**Extended Data Fig. 6**) respectively based on their MS/MS analyses. Co-expression of both enzymes with *Ch*CYP805A11, *Ch*NmrA-1, and *Ch*CYP805A12 in *N. benthamiana* leaves co-infiltrated with **3**, led to consumption of **7** and **8** (including **9**) and production of a new peak ($[H+M]^+$ = *m/z* 314.1387) that was confirmed to be cephalotaxinone (**10**), a *Cephalotaxus* alkaloid[1,17], using LC-MS/MS comparison to a purified cephalotaxinone standard (**Extended Data Fig. 7**). The ability to convert **6** ($[H+M]^+$ = *m/z* 328.1543) to **7** ($[H+M]^+$ = *m/z* 316.1543), and **8** ($[H+M]^+$ = *m/z* 326.1387) to cephalotaxinone ($[H+M]^+$ = *m/z* 314.1387)—both involving a 12 Da loss corresponding to one carbon—demonstrates that *Ch*2OGD-1 is responsible for performing the remarkable carbon excision reaction that contracts ring C to C', a key step in the biosynthesis of CET (**Extended Data Figs. 5 and 7**).

Moreover, conversion of **6** to **8** and **7** to cephalotaxinone illustrated that *Ch*CYP805A13 catalyzes methylenedioxy bridge formation to generate ring E of CET (**Extended Data Figs. 6-7**). When *Ch*CYP805A13 acted on **6**, it produced not only **8** but also **9**, a side-product likely produced by a

330 promiscuous reductase in *N. benthamiana* through reduction of a transient intermediate **9'** that likely
331 arises from reversible ring opening of the tertiary amine in **8** (**Extended Data Fig. 6m**). Formation of **9** is
332 unlikely to result from direct oxidation of **5** by *Ch*CYP805A13, as **9** was not detected in the absence of
333 *Ch*CYP805A12 (**Extended Data Fig. 8**).

334 The five enzymes in *C. harringtonia* identified through co-expression analysis using *Ch*OMT-1
335 as the bait gene establish a biosynthetic pathway of CET from **3** to cephalotaxinone (**Fig. 4** and **Extended**
336 **Data Fig. 8**). The order of the pathway was validated through sequential addition of each enzyme
337 (**Extended Data Fig. 8a-b**) and dropout experiments in which each individual enzyme was removed from
338 the engineered pathway to cephalotaxinone (**Extended Data Fig. 8c**). The sequential accumulation of
339 proposed pathway intermediates with no detection of alternative mass signatures also supported that the
340 overall biosynthetic pathway of CET from **3** to cephalotaxinone is linear, with the final steps involving
341 *Ch*2OGD-1 and *Ch*CYP805A13 may occur in bifurcated sequence (**Extended Data Fig. 8**).
342 Reconstitution of CET biosynthetic pathway from **2** to cephalotaxinone in *N. benthamiana* was also
343 established with co-expression of all the six newly discovered biosynthetic genes in this study and co-
344 infiltration of **2** (**Extended Data Fig. 9**). Furthermore, the identities of all the newly discovered
345 intermediates (**2**, **3**, **5**, **6**, **7**, **8**, and cephalotaxinone) and side-products (**4** and **9**) produced heterologously
346 in *N. benthamiana* were supported by co-elution with metabolites found in *C. harringtonia* root tips that
347 exhibited identical MS/MS fragmentation patterns (**Extended Data Fig. 10**). This indicated that the
348 compounds produced in the *N. benthamiana* expression system are biologically relevant pathway
349 intermediates. In addition to the authentic synthetic or purified standards used to confirm the structures of
350 **2**, **3**, and cephalotaxinone, structural assignments of other proposed intermediates were all supported by
351 LC-MS/MS analyses of the molecules and comparison of their MS/MS fragmentation patterns to those of
352 the corresponding four-deuterated forms from dopamine-$D_4$, **2**-$D_4$, or **3**-$D_4$ feeding study or to those of the
353 related CET biosynthetic intermediates (**Extended Data Figs. 1-10**).

354 Moreover, all the identified intermediates were only observed at high levels in growing root tips
355 of *C. harringtonia* relative to other tissues (**Fig. 4a** and **Extended Data Fig. 9c**). The exception is
356 cephalotaxinone, which is found throughout the plant body. This accumulation of CET intermediates in
357 growing root tips aligned with our findings of the core biosynthesis of HHT (CET) occurring at the root
358 tips. However, the wide distribution of not only CET and HHT (**Fig. 2b**) but also cephalotaxinone (**Fig.**
359 **4a**) throughout the native plant as well as reversible conversion between cephalotaxinone and CET from
360 early radioisotope labeling studies[27] suggests that it is cephalotaxinone that gets primarily made in the
361 growing root tips and is transported throughout the plant. Thus, reduction of cephalotaxinone to CET
362 most likely occurs not only in root tips but also in other tissues, including the aerial part of the plant (**Fig.**
363 **5**). Furthermore, in $D_2O$ labeling studies using excised branches of *C. harringtonia*, there was no
364 detectable enrichment of deuterated cephalotaxinone in needles. In contrast, there was a clear enrichment
365 of deuterated CET and HHT in young needles in these experiments (**Supplementary Fig. 11**).
366 Additionally, enzymes previously characterized in our laboratory that contribute to HHT side-chain
367 biosynthesis, including *Ch*IPMS2 and *Ch*IPMI_SSU2[36] (corresponding to YD-1-Rt_transcript/23102.p1
368 and YD-1-Rt_transcript/44947.p1, respectively), are expressed throughout the plant, with relatively high
369 expression in young needles, young stem, and root tips. These data together support a model (**Fig. 5**) in
370 which the cephalotaxinone alkaloid core is primarily biosynthesized in root tips and subsequently
371 transported throughout the plant body for active reduction to CET (**Supplementary Table 2**). Subsequent
372 side chain tailoring to complete HHT biosynthesis likely occurs in the aerial part of the plant, especially
373 young needles (based on isotope labeling and transcript abundance), and potentially also in root tips
374 (based on transcript abundance).

375 Collectively, we have elucidated a biosynthetic pathway to cephalotaxinone. We discovered six
376 novel biosynthetic enzymes that perform unique transformations, seven pathway intermediates, and two
377 side-products in CET biosynthesis from **2** to cephalotaxinone, which is primarily produced in growing

root tips of *C. harringtonia* and then gets transported throughout the plant for conversion into CET and HHT.

Despite these advances, future investigations are still needed to fully understand the final step of cephalotaxinone to CET and clarify the Pictet-Spengler like reaction to produce the phenethylisoquinoline scaffold in CET biosynthesis. We tested a number of candidate enzymes, including dehydrogenases and reductases, prioritized based on co-expression with the six CET biosynthetic genes that are highly expressed only in root tips of *C. harringtonia* (**Supplementary Fig. 8**), for conversion of cephalotaxinone to CET. However, none of them resulted in production of CET. It is possible that the downstream enzyme(s) responsible for reducing cephalotaxinone to CET may have a significantly different expression pattern relative to early CET biosynthetic genes.

With respect to the formation of the phenethylisoquinoline scaffold in CET biosynthesis, we note that a previous report had described a Bet v 1-like protein (*Ch*PSS) that catalyzes a Pictet-Spengler like reaction in the biosynthesis of compound **1**[29]. Our data support that compound **2** is the likely pathway precursor (**Fig. 2**), and we also were curious about which enzyme(s) enable biosynthesis of this initial phenethylisoquinoline scaffold. We tested a series of putative Bet v 1-like proteins identified through co-expression analysis with *Ch*OMT-1 and a homolog of *Ch*PSS[29] (corresponding to YD-1-Rt_transcript/53915.p1 in our transcriptome with two aa difference). However, these enzymes—heterologously expressed in *N. benthamiana* and assayed using crude leaf protein lysates *in vitro*—do not appear to promote condensation of dopamine with the requisite aldehydes to produce either compound **2** or **1** above slow background levels of condensation (**Supplementary Fig. 12**). In contrast, the previously characterized *Cj*NCS[63] was active in this assay. It is possible that a different enzyme class has evolved in *C. harringtonia* to catalyze this scaffold forming step that remains to be discovered.

## DISCUSSION

Our study demonstrates careful regulation and coordination of biosynthesis of CET, the core scaffold of the ribosome inhibitor HHT, by the plant. *Cephalotaxus* species are slow-growing conifers that follow a seasonal growth cycle, with bud expansion beginning in late March, shoot emergence in late April, and rapid shoot elongation occurring throughout May, followed by winter dormancy[16,37,38]. Our stable-isotope labeled precursor feeding experiments with sectioned tissues of *C. harringtonia* showed that this seasonal cycle strongly influences CET biosynthesis. In tissues collected during active shoot growth in May, incorporation of dopamine-$D_4$ and **2**-$D_4$ into CET-$D_4$ in root tips was observed, whereas sectioned tissues from dormant plants harvested in November and December showed no enrichment of CET-$D_4$ (**Supplementary Table 3**). Furthermore, our *in-house* transcriptome generated from tissues of actively growing *C. harringtonia* collected in May 2023 captured all CET biosynthetic transcripts, whereas our *in-house* transcriptome generated from tissues harvested after the spring growth period (August 2018) had all the CET biosynthetic transcripts missing (**Supplementary Fig. 8**). Although potential limitations of feeding assays and technical errors in RNA sampling from August 2018 cannot be entirely excluded, the consistent detection of CET-$D_4$ enrichment in root tips of an actively growing *C. harringtonia* harvested in May 2022, May 2023, and June 2024, together with transcriptome data from May 2023, supports that CET biosynthesis is seasonally activated during active spring growth, particularly in May and June.

Our findings further illustrate strategic coordination of *C. harringtonia* to produce *Cephalotaxus* alkaloids through whole plant coordination metabolism. The stable-isotope labeled precursor feeding studies and metabolite profiling of various tissues of actively growing *C. harringtonia* revealed that the root tips are the primary site of CET alkaloid core biosynthesis, contrasting with the widespread accumulation pattern of cephalotaxinone, CET, and HHT observed throughout the plant (**Fig. 2** and **Fig. 4a**). The non-toxic cephalotaxinone[1,64] gets synthesized in the growing root tips and transported

425 throughout the plant in an inert form, which can later be reduced to CET[27]—an apparent non-toxic
426 precursor[2,4] poised for esterification with different side-chains to generate toxic defense compounds such
427 as HHT[1,2,4] when and where needed, including young needles (**Fig. 5**). Together, our findings in *C.*
428 *harringtonia* highlights a model in which a plant employs whole-organism metabolic coordination to
429 carefully produce and store toxic defense metabolites, thereby ensuring effective defense while
430 minimizing self-toxicity and unnecessary energy expenditure.

431 It is notable that HHT is one of the few known plant-derived small molecule NPs that inhibit
432 eukaryotic protein translation, whereas most known plant-derived inhibitors of this process are
433 proteins[65,66]. Compared to prokaryotes, far fewer eukaryotic translation inhibitors are known in plants[13,65].
434 Notable plant NPs other than HHT that act as eukaryotic protein translation inhibitors by binding to the
435 large ribosomal subunit include ricin, a protein from castor beans[67], as well as lycorine and narcisclasine,
436 small molecules from *Amaryllidaceae* family[13,65]. Interestingly, *Amaryllidaceae* species have been shown
437 to exhibit spatiotemporal regulation of the biosynthesis of ribosome inhibitor molecules like lycorine[32],
438 which may represent a strategy to mitigate potential autotoxicity—similar to the coordinated CET/HHT
439 biosynthetic pathway observed in *Cephalotaxus*.

440 Our study elucidates the long-elusive biosynthetic pathway to cephalotaxinone—the core alkaloid
441 scaffold of an FDA-approved anti-cancer drug HHT. Stable-isotope labeled precursor feeding, integrated
442 with tissue-resolved metabolite profiling and transcriptomic co-expression analysis, enabled us to identify
443 growing root tips as a site of active HHT alkaloid core biosynthesis, discover seven CET pathway
444 intermediates, and functionally characterize six novel biosynthetic enzymes. Leveraging this paired, *in-*
445 *house* generated metabolomic and transcriptomic dataset across diverse tissues of actively growing *C.*
446 *harringtonia* was critical in fully capturing the spatiotemporally expressed CET biosynthetic genes and
447 identifying co-expressed genes in biosynthetically active tissues, demonstrating a powerful framework for
448 pathway discovery in genetically intractable, slow-growing non-model plants. Furthermore, our findings
449 suggest that *C. harringtonia* employs a sophisticated whole-plant coordination strategy to produce the
450 toxic ribosome inhibitor HHT, offering deeper insights into how certain plants regulate the biosynthesis
451 of eukaryotic ribosomal toxins as a defense mechanism while minimizing autotoxicity. Overall, our work
452 not only establishes a metabolic route to the core scaffold of HHT, enabling future sustainable, large-scale
453 production of this clinically essential drug, but also expands our understanding of whole-plant
454 coordination for biosynthesis of specialized metabolites and the unique biochemical transformations
455 catalyzed by plant enzymes to generate these complex, bioactive molecules.

456

457

458

459

460 **METHODS**

461 *Chemicals and reagents*

462 All biological and chemical reagents were purchased from commercial vendors, unless stated
463 otherwise. These include dopamine (MilliporeSigma), 3-hydroxy-4-methoxyphenethylamine (Combi-
464 Blocks), 3-methoxy-4-hydroxyphenethylamine (Combi-Blocks), 3-(4-hydroxyphenyl)propanal
465 (Chemscene), 3-(3,4-dihydroxyphenyl)propanal (Astatech), 3-(4-hydroxy-3-methoxyphenyl)propanal
466 (Astatech), dopamine-$D_4$ (1,1,2,2-$D_4$; Cambridge Isotope Laboratories), cephalotaxine (Selleckchem), and
467 homoharringtonine (MilliporeSigma).

468

469 *Plant growth*

470 The *Cephalotaxus harringtonia* var. Fastigiata plants used to measure natural abundance of their
471 secondary metabolites and to conduct stable isotope labeled precursor feeding experiments as well as $D_2O$
472 labeling studies were purchased from Forest Farms (forestfarm.com). They were grown in pots with soil,
473 watered approximately once every week. Growth conditions consisted of ambient laboratory temperature
474 and lighting.

475 The *N. benthamiana* plants used for heterologous gene expression were sown and grown in PRO
476 MIX HP Mycorrhizae soil (Premier Tech Horticulture) on growth shelves with a 16/8-h light/dark cycle
477 at ambient laboratory temperature. 4-5 weeks old plants after seeding were used for *Agrobacterium*-
478 mediated transformation.

479

480 *Stable isotope labeled precursor feeding experiments to identify the site of active biosynthesis of CET*

481 Various tissues from *C. harringtonia* var. Fastigiata were excised from the whole plant using
482 ethanol-sterilized scissors. For young inner needles (YIN), actively growing inner young light-green
483 yellowish needles of 0.5-2 cm in length were harvested. Young outer needles (YON) were actively
484 growing outer light-green needles, 1.5-3 cm in length. For young stems (YSt), light-green stems with YIN
485 and YON of 2-3 cm in length from the tip of the stem (meristem) was harvested; all the surrounding
486 needles were removed using a sterile scalpel. Old needles (ON) were mature, dark green needles (≥1-2
487 years old), 4-7 cm in length. For old stems (OSt), at least 1-2 year-old mature dark green stems (4-5 cm in
488 length) with ON removed were collected. Before harvesting root tips (Rt), they were thoroughly washed
489 with water, quickly rinsed with 30% ethanol, and washed again with water as a final washing step. Then,
490 roots of 5-8 cm in length from the root tip, including the root meristem, were collected. Needles and roots,
491 due to their thin structure, were latitudinally split into equally sized sections for paired metabolomics
492 (feeding experiments) and transcriptomics (RNA-seq). Stems were longitudinally sectioned into equal
493 halves for the same paired analyses.

494 Tissues used for accumulated metabolite analysis and RNA extraction were immediately flash
495 frozen in liquid nitrogen and stored at -80 °C until further processing. For feeding experiments, sterile 12-
496 well plates were filled with 2 mL of an aqueous solution of 100 μM dopamine-$D_4$, **1**-$D_4$, **2**-$D_4$, **3**-$D_4$, **12**-
497 $D_4$, or merely deionized water (negative control); see **Supplementary Table 3** for details on when and
498 which experiments were conducted. Each well contained 7-9 needles for YIN, 3 needles for YON, 1 stem
499 for YSt, 3 needles for ON, 1 stem for OSt, and 4-5 roots for Rt, with all tissues cut into smaller pieces to
500 maximize direct contact with the substrate solution. For Rt, the 12-well plates were wrapped in aluminum
501 foil to simulate the darkness experienced by roots growing underground. The assay was conducted for
502 five days, with the solution replaced by freshly prepared substrate solution halfway through (after ~2.5
503 days). Following the remaining ~2.5 days, sectioned tissues were collected into pre-weighed 2 mL
504 Eppendorf Safe-Lock tubes, flash frozen in liquid nitrogen, and lyophilized to dryness. Samples were then
505 processed for analysis using LC-MS (see *Metabolite extraction from plant material and LC-MS analysis*
506 *of metabolites* in Methods). All feeding experiments were performed on tissues from the same plant.

507

508 *$D_2O$ labeling studies and deuterium enrichment analysis*

509 $D_2O$ labeling study with *C. harringtonia* var. Fastigiata was conducted much as previously
510 described[35]. Briefly, two branches (approximately 7 cm in length) were excised from the base of *C.*
511 *harringtonia* var. Fastigiata using ethanol-sterilized scissors and placed cut end down in a Falcon tube
512 containing 10 mL of either 100% deionized water (control) or 10% $D_2O$ in deionized water (prepared
513 from 100% $D_2O$; Sigma-Aldrich). Throughout the experiment, the respective deionized water was

514 replaced every 3-4 days. The caps were placed on the tubes such that airflow could occur. Growth
515 conditions consisted of ambient laboratory temperature and lighting. Both young needles (three needles
516 per sample) at the top end of both branches, which were determined based upon having a lighter green
517 hue, softer needles, and smaller size compared to the rest of the old mature needles, and old needles (two
518 needles per samples) were harvested from both branches treated with either $D_2O$ or $H_2O$ after 5, 10, and
519 15 days of incubation. Three samples were collected at each time point, except the control for old needles
520 that had two samples collected at each time point. All samples were collected into pre-weighed 2 mL
521 Eppendorf Safe-Lock tubes, flash frozen in liquid nitrogen, and lyophilized to dryness. Samples were then
522 processed for analysis using LC-MS (see *Metabolite extraction from plant material and LC-MS analysis*
523 *of metabolites* in Methods).
524 The relative isotope enrichment of *Cephalotaxus* alkaloids, including cephalotaxinone, CET, and
525 HHT, were calculated much as previously described[35]. Briefly, mass isotopologue distributions (MIDs)
526 were obtained by summing MS signal intensities over retention time windows of interest using the
527 **get_MID.py** script from https://github.com/Stanford-
528 ChEMH-MCAC/d2o_metabolomics[35]. From MIDs, isotopic enrichment (IE) was quantified by the
529 following formula:

530 $$\mathrm{IE} = \frac{\sum_{i=0}^{n} \mathrm{M}_i}{n}$$

531 where IE is total heavy isotopic enrichment in the compound, *n* is the number of (integer) mass
532 isotopologues that can be detected, and $M_i$ is the relative abundance of the *i*th isotopologue[35]. Then, for
533 the deuterium enrichment quantitation (the relative isotope enrichment), the IE value of a deuterium-
534 labeled sample was subtracted from the IE value of an unlabeled control sample, correcting for the natural
535 abundance of heavy isotopologues—mainly from $^{13}C$.
536

537 *RNA extraction*

538 Flash-frozen *C. harringtonia* tissues (from May 2023 paired feeding experiments) were
539 homogenized to a fine powder under liquid nitrogen using a chilled mortar and pestle that were pre-
540 treated with RNAse Zap RNAse Decontamination Solution (Thermo Fisher Scientific). RNA from the
541 powdered tissue samples were extracted using RNeasy Plant Mini Kit (Qiagen) with on-column DNase
542 digestion. RLC buffer was used as the lysis buffer. For root samples, the extracted RNA was further
543 cleaned up using the same kit. RNA concentration and purity were measured using a NanoDrop and Qubit
544 (Qubit® 2.0 Fluorometer), and quality was further assessed using an Agilent 2100 Bioanalyzer.

545

546 *Preparation and sequencing of Illumina NovaSeq 6000 libraries and processing*

547 Library preparation for Illumina NovaSeq 6000 (S4 Flow cell – PE150) sequencing was
548 performed using the NEBNext® Ultra™ II RNA Library Prep Kit for Illumina® (non-directional; New
549 England Biolabs), as per the manufacturer instructions. Individual libraries were barcoded with internal
550 index sets at Novogene. For fragmentation, Diagenode Bioruptor Pico was used, and inserts were size
551 selected with NEBNext beads to have an average insert size of 150-200 bp. The PCR products were
552 purified (AMPure XP system). The quality and size distribution of each library were confirmed with
553 analysis using a High Sensitivity DNA chip on a 2100 Bioanalyzer (Agilent). Each library was quantified
554 using Qubit (Qubit® 2.0 Fluorometer) and real-time PCR (Kapa). Equimolar amounts of libraries for each
555 sample (36 total, from May 2023 feeding experiments) were pooled for paired-end sequencing within a
556 single Novaseq 6000 lane (S4 Flow cell – PE150).

557 The quality of raw Illumina sequencing reads was evaluated using FastQC (Babraham
558 Bioinformatics, Babraham Institute). These reads were processed to remove adapters, barcodes, and low-
559 quality sequences using Trimmomatic[68], using the following parameters: <ILLUMINACLIP:TruSeq3-

560 PE-2.fa:2:30:10 LEADING:5 TRAILING:5 SLIDINGWINDOW:4:5 MINLEN:50>. The trimmed reads
561 were then re-assessed with FastQC to confirm quality.

562 While the processed Illumina sequencing reads were used to quantify each transcript abundance
563 against PacBio Iso-Seq transcriptome, we also generated a *de novo* transcriptome assembly from Illumina
564 reads using Trinity[69] with default settings to leverage the higher sequencing depth and broader range of
565 tissues provided through Illumina sequencing, resulting in generation of 541,990 contigs. Quality of the
566 newly assembled transcriptome was assessed by mapping Illumina short reads to the transcriptome using
567 bowtie2[70] and through Benchmarking Universal Single-Copy Orthologs (BUSCO) analysis for
568 completeness[71]. Then, peptide sequences, with longest open reading frame (ORF) identified for each
569 transcript, were predicted using Transdecoder[69], which resulted in 144,299 contigs. Redundant contigs
570 were removed using CD-HIT-EST[72] with 99% identity threshold, yielding a final Illumina *de novo*
571 transcriptome of 102,958 contigs.

572

573 *Preparation and sequencing of PacBio Iso-Seq libraries and processing*

574 Preparation of PacBio Iso-Seq libraries were performed as previously described[39]. For Iso-Seq,
575 only a subset of tissues from the 36 total samples was sequenced: Rt1 (root tips), Rt6 (root tips), an equal
576 combination of Rt4 and Rt8 (root tips), an equal combination of YIN3 and YIN4 (young inner needles),
577 an equal combination of YSt3 and OSt3 (young and old stems), and an equal combination of ON1 and
578 ON2 (old needles). Inclusion of Rt1, Rt,6 and Rt8—tissues with active CET biosynthesis—ensured that
579 the transcriptome contained CET biosynthetic genes. Additional tissues were included to represent all
580 other major tissue types beyond root tips, enabling capture of complete transcripts from *C. harringtonia*.

581 PacBio SMRT library preparation and sequencing were performed by QB3 Genomics, UC
582 Berkeley, Berkeley, CA (RRID: SCR_022170) on the PacBio Sequel II System using the Sequel II 3.1
583 binding kit with a 30-hour movie time. RNA concentration was adjusted to <5 ng/µL using the Qubit HS
584 RNA Kit, and RNA quality was assessed via capillary electrophoresis on an Agilent Bioanalyzer 2100
585 using the Eukaryotic Total RNA Pico Assay, as per the manufacturer instructions, with a 2 min
586 denaturation at 70 °C followed by a 2 min cold shock on ice in a freezer. PacBio SMRT sequencing
587 library was prepared as described in the Iso-Seq™ Template Preparation for Sequel® Systems manual
588 using the NEBNext® Single Cell/Low Input cDNA Synthesis & Amplification Module and the Pacific
589 Biosciences Iso-Seq Express Oligo Kit with the barcoded primers provided in the manufacturer's protocol
590 for first-strand cDNA synthesis (standard purification) and PCR amplification. Barcoded cDNAs from six
591 representative samples (containing 10 unique tissue samples as discussed above) were pooled in
592 equimolar amounts, and a single library was prepared from this pooled cDNA using the SMRTbell Prep
593 Kit 3.0 following the standard protocol. The raw data were then processed using the Iso-Seq 3 pipeline in
594 SMRT® Link software (PacBio) with default settings, resulting in generation of 357,877 high quality
595 transcript isoforms. The quality of the Iso-seq transcriptome was assessed by mapping short read Ilumina
596 short reads to the long read transcriptome assembly using bowtie2[70] and through BUSCO analysis for
597 completeness[71]. Peptide sequences, with longest ORF identified for each transcript, were then predicted
598 using Transdecoder[69], resulting in 349,712 contigs. Redundant contigs were removed using CD-HIT-
599 EST[72] with a cut-off at 99% identity, yielding a final PacBio Iso-Seq transcriptome of 29,163 unique
600 transcripts.

601 For the old *in-house* PacBio Iso-Seq transcriptome—derived from tissues (young and old needles,
602 old stem, and roots) harvested in August 2018 that lack CET biosynthetic genes and used as a comparison
603 to the newly prepared *in-house* transcriptome from tissues harvested in May 2023 (see **Supplementary**
604 **Fig. 8**)—library preparation and sequencing were performed by the Joint Genome Institute (JGI). The
605 2018 dataset was prepared and processed in the same manner as the May 2023 Iso-Seq transcriptome,

606 except for this difference in sequencing facility and usage of CD-HIT-EST cut-off at 98% identity. The
607 final processed transcriptome consisted of 48,657 unique transcripts.

608

609 *Analysis of RNA-seq data*

610 Both the final processed PacBio Iso-seq and *de novo* Illumina-generated transcriptomes (from
611 tissue samples in May 2023) were annotated with best-hit Pfam terms, followed by all subsequent (lower-
612 ranked) Pfam hits[73]. Annotations also included the best Basic Local Alignment Search Tool (BLAST) hit
613 from *Arabidopsis thaliana* proteomes[74] (via UniProt), *Taxus chinensis* proteomes[75], *Cephalotaxus*
614 *hainanensis* proteomes[29], and the *in-house* old Iso-seq transcriptome of *Cephalotaxus harringtonia*
615 (harvested in August 2018), using BLASTP. Quantification of processed Illumina reads against both the
616 PacBio and Illumina-generated transcriptomes was performed using Kallisto[76] with default parameters.
617 For all downstream expression analysis, $\log_2$-transformed, TMM-normalized CPM expression values
618 were used. Ultimately, the PacBio Iso-seq-generated transcriptome (from tissue samples in May 2023
619 paired feeding experiment) was used for all analyses and candidate gene selection to avoid technical
620 limitations of *de novo* Illumina transcriptome assembly (i.e. misassembled or fragmented contigs)[39,40]. For
621 example, *Ch*OMT-1, an essential CET biosynthetic gene we discovered, was detected in the PacBio Iso-
622 seq transcriptome but absent from the *de novo* Illumina assembly.

623

624 *Cloning of candidate biosynthetic genes*

625 cDNA was prepared from extracted RNA of *C. harringtonia* tissues harvested in May 2023 for
626 paired metabolomics and transcriptomics using the SuperScript™ IV First-Strand Synthesis System Kit.
627 Because the candidate biosynthetic genes were highly expressed in root tips tissues, they were cloned
628 mostly from cDNA generated from root tips of *C. harringtonia*. Coding sequences were PCR-amplified
629 using Q5® High-Fidelity DNA Polymerase (New England Biolabs) following the manufacturer's
630 protocol. Oligonucleotide primers were designed to anneal to the 5′ and 3′ ends of the coding sequence for
631 each target gene, incorporating flanking sequences homologous to the intended Gibson assembly sites of
632 the appropriate expression plasmid. Following PCR amplification, the PCR products were assessed using
633 gel electrophoresis on a 1% (w/v) agarose gel. PCR products were either purified using the DNA Clean &
634 Concentrator-5 kit (Zymo Research) prior to transient expression construct assembly or, when necessary,
635 were excised from the gel and purified using the Zymoclean Gel DNA Recovery Kit (Zymo Research).

636 For transient expression construct assembly, pEAQ-HT plasmid was digested with *AgeI and XhoI*
637 restriction enzymes, and PCR amplicons were inserted into the digested pEAQ-HT vector using
638 NEBuilder® HiFi DNA Assembly Mix (New England Biolabs), as per the manufacturer instructions.
639 These Gibson assembly reactions were directly transformed into NEB 10β *Escherichia coli* cells (New
640 England Biolabs) and grown on Luria–Bertani (LB) agar plates containing kanamycin (50 μg/mL)
641 overnight at 37 °C. Positive colonies, with successful insertion of the target gene, were selected by
642 screening with Colony PCR and were used to inoculate 4 mL LB liquid cultures with kanamycin (50
643 μg/mL), which were grown overnight on a rotary drum at 37 °C. Plasmid DNA was isolated using the ZR
644 Plasmid Miniprep Kit (Zymo Research), and the sequences of the inserts were verified by either whole-
645 plasmid sequencing (Plasmidsaurus) or Sanger sequencing (ELIM Biopharm Inc.).

646 pEAQ-HT expression constructs were transformed into *Agrobacterium tumefaciens*
647 (GV3101:pMP90) via the freeze-thaw method. The transformed cultures were grown on LB agar plates
648 containing kanamycin (50 μg/mL) and gentamycin (30 μg/mL) at 30 °C for two days to select positive
649 transformants, which were confirmed by colony PCR. The verified positive colonies were then used to
650 inoculate 2 mL LB liquid cultures (50 μg/mL kanamycin and 30 μg/mL gentamycin), which were grown

651 for two days at 30 °C on a rotary drum and subsequently used to prepare 25% glycerol stocks that were
652 snap-frozen in liquid nitrogen and stored at -80 °C for long-term use.

653

654 *Agrobacterium-mediated transient expression of Cephalotaxus genes in N. benthamiana*

655 Transient expression in *Nicotiana benthamiana* was conducted much as previously described[30,47].
656 Glycerol stocks of *Agrobacterium tumefaciens* strains containing the pEAQ-HT expression construct of
657 interest were streaked onto LB agar plates (kanamycin 50 μg/mL and gentamicin 30 μg/mL), which were
658 then incubated at 30 °C for two days until a dense bacterial lawn developed. The bacterial cells were
659 scraped off with a sterile pipette tip and resuspended in 1 mL of *Agrobacterium* induction buffer (10 mM
660 MES, pH 5.6,10 mM $MgCl_2$, 150 μM acetosyringone; Acros Organics), which were then incubated at
661 room temperature for 1-3 hours. The optical density at 600 nm ($OD_{600}$) was measured for each strain
662 resuspension to determine relative cell density. Individual strain was diluted in induction buffer to an
663 $OD_{600}$ of 0.2-0.3 for infiltration. For transient co-expression, multiple strains of interest were combined in
664 equal concentrations, at a final $OD_{600}$ of 0.2-0.3 for each strain. These individual strains or strain mixtures
665 were infiltrated into the abaxial side of 4-5 week-old *N. benthamiana* leaves using a 1 mL needleless
666 syringe. For each transient expression reaction, three leaves—each from a different plant—were used as
667 biological replicates to minimize any batch effects or biological variations among plants. After 3-4 days
668 of infiltration, 150-250 μL of substrate (25-50 μM of compound **2** or **3** in water) was infiltrated into the
669 abaxial side of previously *Agrobacterium*-infiltrated leaves using a needleless syringe. The area infiltrated
670 with substrate was marked, excised one day after the substrate infiltration, and collected into pre-weighted
671 2 mL Safe-lock tubes (Eppendorf), which were flash frozen in liquid nitrogen and lyophilized to dryness
672 for subsequent metabolite analysis.

673

674 *Preparation of crude protein lysates from N. benthamiana and their in vitro reactions for assessment of*
675 *Pictet-Spengler condensation for phenethylisoquinoline scaffold formation*

676 To evaluate the functionality of candidate enzymes for phenethylisoquinoline scaffold formation
677 in a more controlled environment, cell-free protein lysates were prepared from *N. benthamiana* leaves
678 transiently expressing genes of interest, much as previously described[77]. Briefly, leaves were harvested 4-
679 5 days after infiltration with the *Agrobacterium* strain of interest (1-2 leaves for per sample) and snap
680 frozen in liquid nitrogen. Enzymes were co-expressed for batch testing. The tissue was homogenized
681 using a mortar and pestle with liquid nitrogen. Then, an ice-cold 2 mL Eppendorf tube was filled with the
682 powdered tissue (~1.5 mL), which was resuspended in 1.5 mL of ice-cold Tris buffer (100 mM Tris-HCl
683 pH 7.4, 10% glycerol, 1 mM phenylmethylsulfonyl fluoride and 10 mM $\beta$-mercaptoethanol). The mixture
684 was incubated at 4 °C for 30 min with gentle rocking to facilitate protein extraction. The mixture was then
685 centrifuged at 12,000*g* and 4 °C for 10 min to pellet plant cell debris. The supernatant was removed, and
686 this crude protein lysate was used as the bulk buffer for *in vitro* reactions.

687 Each reaction was carried out in a total reaction volume of 50 μL, containing 1 μL of 2.5 mM
688 dopamine (final concentration, 50 μM), 1 μL of 2.5 mM requisite aldehyde (final concentration, 50
689 μM)—3-(4-hydroxyphenyl)propanal or 3-(4-hydroxy-3-methoxyphenyl)propanal to form **1** or **2**
690 respectively, and 48 μL of the crude protein lysate. The reactions were incubated at 30 °C for 3 h, after
691 which the reactions (50 μL) were quenched by an equal volume (1:1) of acetonitrile with 0.1% formic
692 acid (50 μL) and diluted with 150 μL of methanol to a final volume of 250 μL (a final 5-fold dilution).
693 Samples were then filtered through 0.45 μM hydrophilic PTFE filter plates (MilliporeSigma), and the
694 filtrates were transferred into LC-MS vials for analysis. The remaining unused crude protein lysates were
695 aliquoted (160 μL), snap frozen in liquid nitrogen, and stored at -80 °C.

696

697 *Heterologous expression of ChCYP805A11 in yeast*

698 Expression of *Ch*CYP805A11 in *Saccharomyces cerevisiae* (yeast) was performed as much
699 previously described[30,78]. The coding sequence of *Ch*CYP805A11 was PCR amplified from its pEAQ-HT
700 construct and annealed into BamHI/EcoRI digested pYeDP60 plasmid ($Carb^R$ for *E. coli* selection; *ADE2*
701 for yeast selection) such that the resulting construct contained a C-terminal 6xHis tag through Gibson
702 assembly, as discussed above in cloning of candidate biosynthetic genes. Similarly, the assembled
703 plasmid construct was transformed into NEB 10β *E. coli cells, which were plated for selection on LB*
704 *agar (100* μg/mL carbenicillin) and grown overnight at 37 °C. Positive colonies, verified through colony
705 PCR, were grown on a rotary drum overnight in liquid LB media containing carbenicillin (*100* μg/mL) at
706 37 °C. The plasmid DNA was isolated using the Zymo Miniprep Kit and sequenced through whole-
707 plasmid sequencing (Plasmidsaurus) to confirm the sequence of the inserted gene.

708 The assembled plasmid construct was transformed into chemically competent *S. cerevisiae*
709 WAT11 (*ade*2), which contains a chromosomal copy of the *A. thaliana* cytochrome P450 reductase 1
710 gene (*ATR1*)[79], using the Frozen-EZ Yeast Transformation II Kit (Zymo Research). Positive
711 transformants were selected on synthetic drop-out media plates lacking adenine (6.7g/L yeast nitrogen
712 base without amino acids, 20 g/L glucose, 2 g/L drop-out mix minus adenine [−Ade], 20 g/L agar)[80,81]
713 through growth for 2 days at 30 °C, which were confirmed through colony PCR. A single, positive colony
714 was then used to inoculate a 4 mL of liquid cultures of synthetic drop-out medium, grown for 2 days at 30
715 °C with shaking at 250 rpm. The liquid cultures were then used to prepare 25% glycerol stocks and stored
716 at -80 °C for long-term usage.

717 Freshly streaked colonies from *S. cerevisiae* WAT11 strain of interest (harboring pYeDP60
718 plasmid of *Ch*CYP805A11) were inoculated in 4 mL of liquid cultures of synthetic drop-out media (-Ade)
719 and were grown at 30 °C for 2 days with shaking at 250 rpm. Then, 2 mL of the starter culture was used
720 to inoculate 500 mL of the synthetic drop-out media (-Ade) and grown at 28 °C with 250 rpm shaking
721 until reaching a cell density of approximately 5 x $10^7$ cells/mL, estimated through $OD_{600}$ measurements.
722 At this density, gene expression was induced by adding 50 mL of a sterile galactose solution (200 g/L) to
723 a final concentration of 10% (v/v). The culture was grown for another 18 h at 28 °C and 250 rpm to reach
724 a cell density of 5 x $10^8$ cell/mL, which was immediately used for microsomal protein isolation.
725 Moreover, other than *Ch*CYP805A11 with C-terminal 6xHis tag, a negative control of empty vector and
726 *Ch*CYP805A11 without His-tag (a negative control for immunoblotting) were prepared as well.

727

728 *Isolation of ChCYP805A11-enriched microsomes from yeast*

729 Yeast microsomal proteins were isolated from yeast following a previously described protocol[78].
730 The galactose-induced yeast cultures were centrifuged at 5,000*g* for 5 min at 4° C to pellet cells. The cells
731 were then resuspended in 1 mL of ice-cold TEK buffer (50 mM Tris-HCl, 1 mM EDTA, 100 mM KCl,
732 pH 7.4) per 0.5 g of wet cell pellet mass and incubated at room temperature for 5 min The cells were
733 centrifuged again as above and resuspended in 5 mL ice-cold TES B buffer (50 mM Tris-HCl, 1 mM
734 EDTA, 600 mM sorbitol, pH 7.4). All subsequent steps were performed at 4 °C and/or on ice.
735 Approximately 5 mL (a volume equal to that of the cell resuspensions) of glass beads (0.5 mm diameter)
736 was added to the cells, which were lysed by vigorous shaking for 10 min (30 s of shaking followed by 30
737 s on ice to avoid heating). Next, 10 mL of ice-cold TES B buffer was added to the lysate, which was then
738 removed from the beads and saved. To extract any residual microsomal proteins on the beads, the beads
739 were washed twice with 10 mL TES B buffer, and all washes were combined with the initial lysate (~30
740 mL total). This pooled lysate was centrifuged at 23,000*g* for 10 min at 4 °C to pellet and remove large
741 cell debris, and the resulting supernatant (~30 mL) was diluted two-fold with ice-cold TES B buffer (to a

742 final volume of ~60 mL). Microsomes were precipitated by adding NaCl to a final concentration of 150
743 mM and polyethylene glycol (PEG)-4000 to a final concentration of 0.1 g/mL, followed by incubation on
744 ice for about 1 h with periodic mixing to dissolve the solutes. Microsomal proteins were then pelleted by
745 centrifugation at 10,000*g* for 10 min at 4 °C and were resuspended in 1 mL of ice-cold TEG storage
746 buffer (50 mM Tris-HCl, 1 mM EDTA, 20% (v/v) glycerol, pH 7.4). The protein concentration of the
747 microsomal fraction was measured using Bradford Assay, and 50-100 µL aliquots were snap-frozen in
748 liquid nitrogen and stored at -80 °C until usage.

749

750 *Immunoblotting (Western blot)*

751 Purified yeast microsomes expressing *Ch*CYP805A11 with a C-terminal 6-His tag,
752 *Ch*CYP805A11 without a His-tag, or empty vector were each loaded into individual wells of a precast
753 polyacrylamide gel (4–15% Mini-PROTEAN® TGX™ Precast Protein Gels, 12-well, 20 µl; Bio-
754 Rad 4561085). Proteins were separated for a total of 55 minutes (50 V for 10 min, followed by 150 V for
755 45 min) and transferred onto a polyvinylidene difluoride (PVDF) membrane using a Bio-Rad Trans-Blot
756 Turbo Transfer System (Bio-Rad, 1704150). Membranes were incubated with horseradish peroxidase
757 (HRP)-conjugated anti-His tag antibody (1:1,000 dilution; Biolegend) for 2 h at room temperature with
758 gentle rocking. Blots were then washed and imaged using an iBright FL1500 Imaging System
759 (Invitrogen, a44241). The microsomes were also analyzed for protein content by sodium dodecyl sulfate
760 polyacrylamide gel (SDS-PAGE) with Coomassie Blue staining (see **Extended Data Fig. 3b** for both the
761 immunoblot and the protein gel).

762

763 *Heterologous production and purification of ChNmrA-1*

764 For heterologous production and purification of *Ch*NmrA-1, the gene was expressed in *E. coli*.
765 The coding sequence of *Ch*NmrA-1 was first PCR amplified from its pEAQ-HT construct and inserted
766 into NdeI/XhoI digested pET-24b ($Km^R$) plasmid such that the resulting construct contained a C-terminal
767 6xHis tag through Gibson assembly, as discussed above in cloning of candidate biosynthetic genes.
768 Similarly, the assembled plasmid construct was transformed into NEB 10β *E. coli cells, which were*
769 *plated for selection on LB agar (50* µg/mL kanamycin) and grown overnight at 37 °C. Positive colonies,
770 verified through colony PCR, were grown on a rotary drum overnight in liquid LB media containing
771 kanamycin (*100* µg/mL) at 37 °C. The plasmid DNA was isolated using the Zymo Miniprep Kit and
772 sequenced through whole-plasmid sequencing (Plasmidsaurus) to confirm the sequence of the inserted
773 gene. The verified plasmid DNA was then transformed into *E. coli* BL21 (DE3) cells (NEB) as an
774 expression host for heterologous protein production. A single positive colony confirmed via colony PCR
775 was then inoculated in 3 mL of LB media (*50* µg/mL kanamycin) and grown overnight on a rotary drum
776 at 37 °C, which was used to prepare 25% glycerol stocks that were snap-frozen in liquid nitrogen and
777 stored at -80 °C for future use.

778 Freshly streaked colonies from *E. coli* BL21 strains of interest (harboring pET-24b of *Ch*NmrA-
779 1) were inoculated in 2 mL of liquid LB cultures (*50* µg/mL kanamycin) and grown overnight on a rotary
780 drum at 37 °C. A 500 µL of the starter culture was inoculated in 200 mL of liquid LB culture containing
781 kanamycin (*50* µg/mL), which was grown on a culture shaker at 37 °C with 250 rpm until $OD_{600}$ of ~0.6
782 was reached. Once reached, the temperature was reduced to 18 °C and shaken for 0.5-1 h, followed by 0.5
783 mM IPTG induction. The cultures were shaken at 250 rpm for 18-20 h at 18°C and then centrifuged at
784 5,000 rpm for 10 min at 4 °C to pellet the cells. All subsequent steps were performed on ice and/or at 4
785 °C. The cell pellets (~1-2 g) were resuspended in 5-8 mL of ice-cold binding buffer (50 mM potassium
786 phosphate, pH 7.8, 100 mM NaCl, 10 mM imidazole) and lysed using EmulsiFlex®-B15 High-Pressure

787 Homogenizer with pressure at 15,000 psi; samples were homogenized three times to ensure full lysis of
788 the cells. Cell lysates were centrifuged at 10,000*g* for 30 min at 4 °C to pellet cell debris.

789 For protein purification, the clarified lysate was added to Ni-NTA resin (Ni-NTA Agarose,
790 Invitrogen; R901-15) and incubated at 4 °C for 1 hour with gentle rocking. Bound proteins were eluted
791 sequentially using potassium phosphate buffer (50 mM potassium phosphate, 100 mM NaCl, pH 7.8) with
792 increasing concentrations of imidazole. Each eluted fraction was analyzed for protein content by SDS-
793 PAGE with Coomassie Blue staining (see **Extended Data Fig. 3c** for the protein gel). Fractions
794 containing pure enzyme were combined and concentrated using Amicon® Ultra-15 Centrifugal Filter
795 Units (10 kDa molecular weight cut-off) by centrifugation at 4,000*g* for 20 min at 4 °C. The unfiltered
796 protein-containing solution (concentrated to <1 mL) was diluted with 10-13 mL of ice-cold potassium
797 phosphate buffer and reconcentrated as above; this dilution-concentration cycle was repeated 6-8 times to
798 dilute out imidazole. The final concentrated protein solution was diluted to approximately 1 mL with ice-
799 cold phosphate buffer, which had glycerol added to a final concentration of 10% (v/v). The purified
800 protein concentration as measured using Bradford Assay, and 30 μL aliquots were snap-frozen in liquid
801 nitrogen and stored at -80 °C for future use.

802

803 *In vitro reactions with purified ChNmrA-1 and ChCYP805A11-enriched microsomes*

804 *In vitro* reactions with purified *Ch*NmrA-1 and *Ch*CYP805A11-enriched microsomes were
805 carried out in 200 μL of potassium phosphate buffer (50 mM potassium phosphate, 100 mM NaCl, pH
806 7.8) with a final concentration of 50 μM of initial substrate (compound **3**) and 1 mM NADPH. Purified
807 *Ch*NmrA-1 (6xHis-tagged) and yeast microsomal proteins containing *Ch*CYP805A11 (6xHis-tagged)
808 were each added to a final concentration of 0.4 μg/μL in a total reaction volume of 200 μL. As negative
809 controls, microsomal fractions containing empty vector (EV) and denatured (boiled) *Ch*NmrA-1 were
810 used. Dependence of the reaction on both the substrate (**3**) and cofactor (NADPH) was also demonstrated
811 through dropping out each component. The reactions were incubated at 30 °C for several time points (0.5,
812 2, and 4 h). The reaction aliquots (20 μL) were then quenched by an equal volume (1:1) of methanol (20
813 μL), followed by addition of an equal volume (1:1) of ice-cold acetonitrile with 0.1% formic acid (40
814 μL). Samples were further diluted with 120 μL of ice-cold methanol to a final volume of 200 μL (2:3,
815 v/v). In parallel, to probe the structure of compound **4'**, proposed to be an unstable imine intermediate, a
816 20 μL aliquot taken from the same 200 μL *in vitro* reaction was not immediately quenched with
817 methanol, but instead treated with an equal volume (1:1) of 100 mM $NaBD_3CN$ in acetate buffer (200
818 mM sodium acetate, pH 5.5) and incubated for 15 min at room temperature to chemically (non-
819 enzymatically) reduce the imine of **4'** to the corresponding amine, yielding monodeuterated **5** (**5**-D)[60].
820 The resulting reactions (40 μL) were quenched with an equal volume (1:1) of ice-cold acetonitrile with
821 1% formic acid (40 μL), followed by dilution with 120 μL of ice-cold methanol to a final volume of 200
822 μL (2:3, v/v). All quenched samples were vortexed and centrifuged briefly. The resulting supernatants
823 were filtered through 0.45 μM hydrophilic PTFE filter plates (MilliporeSigma), and the filtrates were
824 transferred into LC-MS vials for analysis.

825

826 *Metabolite extraction from plant material*

827 The overnight-lyophilized tissues (i.e. various tissues of *C. harringtonia* from feeding
828 experiments and leaves from *N. benthamiana* transient expression experiments) were homogenized on a
829 ball mill homogenizer (Retsch MM 400) using a 5 mm diameter steel bead for each sample tube, with
830 shaking at 25 Hz for 2 min Steel beads were then removed, and each tissue sample was extracted with 40
831 μL and 20 μL of 80% methanol in water per milligram of dry plant tissue weight for *C. harringtonia*

832 tissues and *N. benthamiana* leaves, respectively. The samples were briefly vortexed and sonicated, then
833 incubated for 30 min at room temperature for metabolite extraction. For *C. harringtonia* tissues,
834 additional 20 min of incubation at 4 °C was performed. The extracted samples were centrifuged at
835 16,000*g* for 1 min to pellet plant cell debris, and the supernatant was filtered through hydrophilic PTFE
836 filter plates with 0.45 μM pore size (MilliporeSigma). The filtrates were transferred into LC-MS vials for
837 analysis.

838 For quantification of natural abundance of cephalotaxinone, CET, and HHT, a 1000-fold and 200-
839 fold dilution was performed for tissues harvested in May 2022 and May 2023 respectively to avoid
840 saturation of the parent isotope peaks in LC-MS. For tissues harvested from $D_2O$ labeling assays
841 (conducted in late April 2022), additional 100-fold dilution was also performed to avoid saturation of the
842 parent isotope peaks in LC-MS.

843

844 *LC-MS analysis of metabolites*

845 All metabolite samples were analyzed on the LC-MS instrument of an Agilent 1290 Infinity II
846 UHPLC coupled to an Agilent 6546 Q-TOF mass spectrometer (6546 LC-MS). For separation of the
847 metabolites, a reversed-phase liquid chromatography using a ZORBAX RRHD Eclipse Plus 95Å C18
848 column (Agilent, 2.1 x 50 mm, 1.8 μm) was performed with a mobile phase consisting of two buffers:
849 water with 0.1% formic acid (buffer A) and acetonitrile with 0.1% formic acid (buffer B). An injection
850 volume of 1 μL and a flow rate of 0.6 mL/min were used with the following 29 min gradient method: 0-
851 0.5 min, 3% B; 0.5-7.5 min, 3-10% B; 7.5-15.5 min, 10-25% B; 15.5-20.5 min, 25-50% B; 20.5-21.5 min,
852 50-95% B; 21.5-23.0 min, 95% B; 23.0-24.5 min, 95-30% B; 24.5-26.5 min, 30-3% B; 26.5-29.0 min, 3%
853 B. MS data were collected using a dual-inlet Agilent Jet Steam electrospray ionization (Dual AJS ESI) in
854 positive ion mode with a mass range of 50-1,700 *m/z* and a rate of 1.00 spectrum per second (1000 ms per
855 spectrum). The ionization source was set as follows: 325 °C gas temperature, 10 L/min drying gas, 35 psi
856 nebulizer, 350 °C sheath gas temperature, 12 L/min sheath gas flow, 135 V fragmentor, 45 V skimmer,
857 750 V Oct 1 RF Vpp, 4000 V VCap, and 0 V nozzle voltage. For tandem mass spectrometry (MS/MS)
858 analysis, the mass ions pertaining to individual metabolites were fragmented with collision energies of 15,
859 20, 30, or 35 V. All data were collected in centroid mode, but when needed, data were also stored in
860 profile mode. Metabolite samples from *in vitro* reactions were analyzed using a shortened gradient
861 method in which the first 7.5 min were identical to the standard long gradient method; all relevant
862 metabolites in *in vitro* reactions (including compounds **4** and **5**) eluted within this window, with
863 compound **3** eluting shortly thereafter (~7.8 min)—resulting in the same elution behavior as observed
864 with the long gradient method. The remainder of the shortened gradient was as follows: 7.5-9 min, 10-
865 50% B; 9-10 min, 50-95% B; 10-11.5 min, 95% B; 11.5-12.5 min, 95-3% B; 12.5-15 min, 3% B.

866

867 *Metabolomics and MS data analyses*

868 LC-MS data were analyzed using Agilent MassHunter Qualitative Analysis 10.0 and Agilent
869 MassHunter Quantitative Analysis 11.0 software. The ion abundances for a given mass signature were
870 calculated using the automated integration ('Agile' method with default settings) of extracted ion
871 chromatograms (EICs) with a 20 ppm mass tolerance. Peaks integrated by the Quantitative Analysis
872 software were manually inspected to ensure correct peak selection and integration.

873 Untargeted metabolomic analyses were conducted using XCMS Online[82] with default parameters
874 of UPLC / UHD Q-TOF (155). The output of this analysis contains a tabulated list of identified mass
875 signatures at specific retention times, with associated *m/z* values, peak intensity fold change, *P* value
876 (two-tailed unequal variance Welch's *t*-test), retention times, and extracted peak intensities.

877 For XCMS analysis comparing dopamine-$D_4$-fed root tips with water-fed controls of *C.*
878 *harringtonia* from isotope labeled precursor feeding studies, we used the following filters to look for
879 differential mass signatures: *P* value < 0.2, fold change > 3.5, and *m/z* range of in between 200 and 600.

880 For XCMS analysis to determine masses found at differential levels between two samples from
881 *N. benthamiana* transient expression experiments, we used the following filters, unless stated otherwise:
882 *P* value < 0.1, fold change > 5, average peak intensity > $5x10^4$, retention time < 18 min, and 250 < *m/z* <
883 600.

884 For XCMS analysis to determine masses found at differential levels between two samples from *in*
885 *vitro* experiments, we used the same filters as above for *N. benthamiana* transient expression experiments,
886 with the exception of the retention time window, which was modified to accommodate the shortened
887 gradient (< 10 min).

888

889 *Synthesis of different phenethylisoquinolines (**1**, **1**-$D_4$, **2**, **2**-$D_4$, **3**, **11**, **12**, **12**-$D_4$, and **13**)*

890 The synthesis of compound **1** (1-(4-hydroxyphenethyl)-1,2,3,4-tetrahydroisoquinoline-6,7-diol)
891 was adapted from a previously described protocol[83]. Dopamine (0.42 mmol) and of 3-(4-
892 hydroxyphenyl)propanal (0.50 mmol) were combined in 4 mL of a 1:1 (v/v) mixture of acetonitrile and
893 potassium phosphate buffer (0.1 M, pH 6.0). The reaction mixture was stirred at 50 °C for 16 h under $N_2$
894 with reflux. The mixture was then frozen in liquid-nitrogen and lyophilized to dryness.

895 The above procedure was applied to the synthesis of all compounds listed in Table 1 below,
896 substituting the amine and aldehyde starting materials as specified.
897
898 **Table 1.** Synthesis of phenethylisoquinolines

| Compound | Amine (0.42 mmol) | Aldehyde (0.50 mmol) |
|---|---|---|
| **1** | dopamine | 3-(4-hydroxyphenyl)propanal |
| **1**-$D_4$ | dopamine-$D_4$ | 3-(4-hydroxyphenyl)propanal |
| **2** | dopamine | 3-(4-hydroxy-3-methoxyphenyl)propanal |
| **2**-$D_4$ | dopamine-$D_4$ | 3-(4-hydroxy-3-methoxyphenyl)propanal |
| **3** | 3-hydroxy-4-methoxyphenethylamine | 3-(4-hydroxy-3-methoxyphenyl)propanal |
| **11** | 3-hydroxy-4-methoxyphenethylamine | 3-(4-hydroxyphenyl)propanal |
| **12** | dopamine | 3-(3,4-dihydroxyphenyl)propanal |
| **12**-$D_4$ | dopamine-$D_4$ | 3-(3,4-dihydroxyphenyl)propanal |
| **13** | 3-methoxy-4-hydroxyphenethylamine | 3-(3,4-dihydroxyphenyl)propanal |

899 For compounds **1**, **1**-$D_4$, **11**, **12**, **12**-$D_4$, and **13**, the lyophilized crude product was resuspended in
900 ~1-2 mL of DMSO and directly loaded onto a Biotage® Sfär C18 D Duo 100 Å 30 µm 6 g column.
901 Purification was performed an automated Biotage Selekt system using water with 0.1% formic acid and
902 acetonitrile with 0.1% formic acid as mobile phases. Eluting fractions containing the compound of
903 interest (identified by LC-MS) were pooled, frozen in liquid nitrogen, and lyophilized to dryness.

904 For compounds **2**, **2**-$D_4$, and **3**, the lyophilized crude product was resuspended in ~2-3 mL of 80%
905 MeOH and purified by preparative HPLC using an Agilent 1260 Infinity preparative-scale HPLC system
906 with an Agilent 1100 diode array detector and a Clipeus C18 5-µm, 10-mm x 250-mm semi-prep column
907 (Higgins Analytical). Water with 0.1% formic acid (A) and acetonitrile with 0.1% formic acid (B) were
908 used as the mobile phases.

909 For compounds **2** and **2**-$D_4$, an injection volume of 500 μL and a flow rate of 5 mL/min were
910 used with the following gradient method: 0-5 min, 3% B; 5-8 min, 3-10% B; 8-23 min, 10-20% B; 23-24
911 min, 20-25% B; 24-24.1 min, 25-97% B; 24.1-29.1 min, 97% B; 29.1-29.2 min, 97-3% B; 29.2-34 min,
912 3% B. Fractions were collected from 1-34 min, and those containing the compound of interest (verified by
913 LC-MS) were combined, frozen, and lyophilized to dryness.

914 For compound **3,** an injection volume of 500 μL and a flow rate of 5 mL/min were used with the
915 following gradient method: 0-5 min, 3% B; 5-8 min, 3-16% B; 8-18 min, 16-24.5% B; 18-19 min, 24.5-
916 30% B; 19-19.1 min, 30-97% B; 19.1-24.1 min, 97% B; 24.1-24.2 min, 97-3% B; 24.2-29 min, 3% B.
917 Fractions were collected from 1-29 min, and those containing the desired compound (verified by LC-MS)
918 were pooled, frozen, and lyophilized to dryness.

919 All the purified products **1**, **1**-$D_4$, **2**, **2**-$D_4$, **3**, **11**, **12**, and **12**-$D_4$ were analyzed by both LC-MS/MS
920 and NMR. For compound **13**, its structure was verified by LC-MS/MS.

921

922 *Heterologous production and purification of compound 3-$D_4$ using ChOMT-1*

923 Compound **3**-$D_4$ was biosynthesized from chemically synthesized **2**-$D_4$ by heterologous
924 expression of *Ch*OMT-1 in *E. coli* BL21 (DE3). Cloning and expression of *Ch*OMT-1 were performed
925 exactly as described for *Ch*NmrA-1 (see Methods: *Heterologous production and purification of ChNmrA-*
926 *1*), except that the induction culture volume was increased to 900 mL. After 18 h of 0.5 mM IPTG
927 induction of *Ch*OMT-1 at 18 °C with shaking at 250 rpm, compound **2**-$D_4$ was added to a final
928 concentration of 50 μM for O-methylation reaction of **2**-$D_4$ to **3**-$D_4$. The biosynthetic reaction was run for
929 5 h with continuous shaking of 250 rpm at 18 °C. The bacterial cells were pelleted, resuspended in 900
930 mL of fresh LB media, and subjected to two additional cycles of the O-methylation reaction (total of three
931 900 mL reactions). The combined supernatants containing the biosynthesized **3**-$D_4$ were extracted with
932 ethyl acetate (1:1, v/v) four times. Organic phases were combined, dried using rotary evaporation, and
933 resuspended in ~3 mL of 80% MeOH. Purification was performed using the same preparative HPLC
934 system, column, and mobile phases as described for compounds **2**, **2**-$D_4$, and **3**, but with a modified
935 gradient method.

936 For compound **3**-$D_4$**,** an injection volume of 200 μL and a flow rate of 5 mL/min were used with
937 the following gradient method: 0-5 min, 3% B; 5-8 min, 3-9.5% B; 8-16 min, 9.5% B; 16-21 min, 9.5-
938 11% B; 21-36 min, 11% B; 36-41 min, 11-13% B; 41-44 min, 13-16%; 44-46 min, 16-20 min; 46-47 min,
939 20-30%; 47-47.1 min, 30-97%; 47.1-52.1 min, 97% B; 52.1-52.2 min, 97-3% B; 52.2-57 min, 3% B.
940 Fractions were collected from 1-57 min, and those containing the compound of interest (verified by LC-
941 MS) were combined, frozen, and lyophilized to dryness. The purified product **3**-$D_4$ was then analyzed by
942 LC-MS/MS and NMR.

943

944 *Extraction and purification of a cephalotaxinone (**10**) standard*

945 Old leaves and stem of *C. harringtonia* were harvested, frozen at -80 °C, and lyophilized to
946 dryness. The dried tissues (~10 g) were then ground to a fine powder or small pieces using mortar and
947 pestle, and extracted with 700 mL of methanol for 3-4 days at room temperature with constant stirring.
948 Extracts were filtered using vacuum filtration and dried by rotary evaporation. Because the compound of
949 interest (CET intermediate) is alkaloid, an acid-base extraction was performed to remove water-soluble
950 and non-alkaloid impurities prior to two rounds of chromatography. The residue was resuspended in 450
951 mL of water with HCl (pH 2-3). This fraction was partitioned with 400 mL of diethyl ether or *tert*-butyl
952 methyl ether. The aqueous fraction was collected, and the organic phase was washed twice with 100 mL
953 of water (pH 2-3) to maximize extraction of the desired compound, after which each of these aqueous

954 fractions was combined with the initial 450 mL aqueous fraction. Then, the pH of the aqueous phase was
955 increased to pH 8-9 using saturated sodium bicarbonate. This solution was partitioned with 600 mL of
956 ethyl acetate. The organic layer, which supposedly contains the target compound, was collected,
957 combined with two additional 100 mL ethyl acetate fractions used to wash the aqueous phase, and dried
958 using rotary evaporation.

959 The dried residue was resuspended in ~1-2 mL of methanol and loaded onto a 3.5 cm-diameter
960 column packed with 18 g of P60 silica gel (SiliCycle). Hexane (HPLC grade; VWR) and ethyl acetate
961 (ACS reagent grade; J.T. Baker) were used as mobile phases. The following gradient was applied: 100
962 mL each of 50%, 60%, 70%, 80%, 90%, and 100% ethyl acetate. Each step was collected in three
963 fractions, yielding a total of 18 fractions. Fractions containing the compound of interest (identified by LC-
964 MS) were combined and dried by rotary evaporation. The partially purified product was resuspended in
965 ~3-4 mL of 80% MeOH for second round of chromatography.

966 For the second round, purification was performed using the same preparative HPLC system,
967 column, and mobile phases as described for compounds **2**, **2**-$D_4$, and **3**, but with a modified gradient
968 method. An injection volume of 450 µL and a flow rate of 5 mL/min were used with the following
969 gradient method: 0-5 min, 3% B; 5-8 min, 3-7% B; 8-10 min, 7% B; 10-13 min, 7-10% B; 13-16 min,
970 10% B; 16-20 min, 10-15% B; 20-24 min, 15%; 24-30 min, 15-25 min; 30-37 min, 25-40%; 37-37.1 min,
971 40-97%; 37.1-42.1 min, 97% B; 42.1-42.2 min, 97-3% B; 42.2-47 min, 3% B. Fractions were collected
972 from 1-47 min, and those containing the compound of interest (confirmed by LC-MS) were combined,
973 frozen, and lyophilized to dryness.

974

975 *NMR analysis of purified compound*

976 DMSO-$d_6$ (ThermoFisher Scientific) was used as the solvent for all NMR samples of
977 phenethylisoquinolines (**1**, **1**-$D_4$, **2**, **2**-$D_4$, **3**, **3**-$D_4$, **11**, **12**, and **12**-$D_4$). For NMR sample of
978 cephalotaxinone (**10**), $CDCl_3$ (Acros Organics) was used as the solvent. $^1H$, $^{13}C$, and 2D-NMR spectra
979 were mostly acquired on a Bruker NEO 500-MHz spectrometer, and on a Varian Inova 600-MHz (for
980 ROESY for **10**) at room temperature using VNMRJ 4.2. The data were visualized, analyzed, and
981 processed on MestReNova v.15.1.0. Chemical shifts were reported in ppm downfield from $Me_4Si$ by
982 using the residual solvent peak as an internal standard: 7.26 ppm for $^1H$ and 77.16 ppm for $^{13}C$ ppm
983 chemical shift of $CDCl_3$ and 2.50 ppm for $^1H$ and 39.52 ppm for $^{13}C$ ppm chemical shift of DMSO-$d_6$.

984 The NMR spectra for compounds **1**, **1**-$D_4$, **2**, **2**-$D_4$, **3**, **3**-$D_4$, **11**, **12**, **12**-$D_4$, and cephalotaxinone
985 (**10**) are shown in **Supplementary Figs. 13-63**, and their $^1H/^{13}C$ assignments are detailed in
986 **Supplementary Tables 6-15**.

987

988 *Sequence analysis of NmrA-like proteins and construction of their phylogenetic tree*

989 Sequence analyses of NmrA-like proteins (atypical SDRs) and related enzymes were performed
990 in Geneious (v2022.2.1). To generate protein alignments of NmrA-like proteins (atypical SDRs), an
991 assortment of protein sequences with PFAM (PF05368), containing the $NAD(P)^+$/NAD(P)H-binding
992 motif, was downloaded from UniProt (https://www.uniprot.org/), Phytozome (https://phytozome-
993 next.jgi.doe.gov/), and NCBI database (https://www.ncbi.nlm.nih.gov/). NmrA-like proteins (PF05368)
994 from high-quality plant genomes, top 2 best BLASTP hits of *Ch*NmrA-1 in the NCBI database, enzymes
995 with verified reductase activity in plant biosynthesis such as the pinoresinol-lariciresinol reductases
996 (PLRs) in lignan biosynthesis (PF05368) and classical SDRs (PF00106), and NmrA-like proteins
997 (PF05368) with verified regulatory functions such as transcription repressors or redox sensor proteins
998 from animals, fungi, and bacteria were selected. Another NmrA-like protein from *C. harringtonia* (YD-1-

Rt_transcript/51169.p1) was also included for analysis, which was identified using best reciprocal BLASTP analysis: *Ch*NmrA-1 was used as a query against the selected high-quality plant genomes, and the top hits were then queried back against our *C. harringtonia* transcriptome. *Ch*NmrA-1 was used as the reference for amino acid numbering in alignments, as it represents the focal NmrA-like protein investigated in this study. Classical SDRs, including SDR1 from *A. thaliana* (UniProt ID: Q9M2E2)[84,85], were included as canonical enzymatic references for comparison of the NAD(P)H-binding motif[55,86]. All sequences were downloaded from UniProt, except the protein from *T. lanceolata* (accession number, XP_077234198.1) and *Pt*SDR-2 from *P. tetrastichus* (GenBank accession number, OR538109) which were downloaded from NCBI database. The downloaded sequences were aligned using MAFFT[87], and the phylogenetic tree was constructed using FastTree[88] with a rate of categories of sites as 20 and an optimization of the Gamma20 likelihood.

*General software use and graph generation*

Routine data compilation was performed in Microsoft Excel (version 16.62), including calculation of Pearson's correlation coefficient used for co-expression analysis. General LC-MS data analysis was performed with Agilent MassHunter Qualitative Analysis 10.0. Chromatograms and mass spectra were plotted using IGOR Pro (version 8.04). Bar graphs, lines graphs, and scatterplots were plotted using GraphPad Prism 10, including mean and standard deviations denoted in the graphs. Geneious Prime (v2022.2.1) was used for bioinformatic analyses of nucleic acid and protein sequences. This software was also used for several sequence alignments (MAFFT)[87] and phylogenetic tree generation (FastTree)[88]. NMR data were processed and visualized on MestReNova v15.1.0. Molecular weight calculation, and chemical structural visualization were conducted using ChemDraw Professional v25.0.2.

*Data Availability*

The raw RNA-seq data analyzed and used for discovery (*C. harringtonia* tissues harvested in May 2023) have been deposited in the National Center for Biotechnology Information (NCBI) Sequence Read Archive (SRA) database under the BioProject ID PRJNA1395191. The processed RNA-seq data, including both the processed PacBio Iso-seq transcriptome and a sheet of expression values (in $\log_2$-transformed values of each transcript calculated as TMM-normalized CPM) for all 29,163 transcripts, analyzed and used for discovery have been deposited at the NCBI Gene Expression Omnibus (GEO) (accession GSE319274). Gene sequences for enzymes characterized in this study have been deposited in the NCBI GenBank under the following accessions: *Ch*OMT-1 (PX794901), *Ch*CYP805A11 (PX794902), *Ch*NmrA-1 (PX794903), *Ch*CYP805A12 (PX794904), *Ch*CYP805A13 (PX794905), and *Ch*2OGD-1 (PX794906). The UniProt database (https://www.uniprot.org/), Phytozome database (https://phytozome-next.jgi.doe.gov/), and NCBI database (https://www.ncbi.nlm.nih.gov/) were used for identifying and obtaining NmrA-like protein sequences that were used in phylogenetic analyses. All other raw/source data are available upon request.

## ACKNOWLEDGEMENTS

We thank Stephen Lynch (Stanford University) for his assistance and helpful discussion related to NMR analysis. We also thank Prof. David Nelson (University of Tennessee) for providing cytochrome P450 nomenclature. We acknowledge Prof. George Lomonossoff for providing us with the pEAQ-HT plasmid. We are grateful to Warren Lau and Catherine Liou for early contributions to this project. The author is also thankful to Diego Wengier and Sarah Niehs for feedback on this manuscript. An initial *C. harringtonia* transcriptome (August 2018) (proposal: 10.46936/10.25585/60001097 led by J. Bohlmann) was performed by the US Department of Energy (DoE) Joint Genome Institute (https://ror.org/04xm1d337), a DoE Office of Science User Facility, and is supported by the Office of Science of the US DoE operated under contract number DE-AC02-05CH11231. The research is supported by an NIH R01 GM121527 to E.S.S.

## AUTHOR CONTRIBUTIONS

**Y.D.** and **E.S.S.** led the project and conceived of experimental procedures. **Y.D.** performed the experiments, generated the new *C. harringtonia* transcriptome (May 2023) used for discovery, and analyzed the data. **K.S.** collected the samples for the initial *C. harringtonia* transcriptome (August 2018) for seasonal comparison and helped develop the hypothesis for a whole plant coordination of HHT biosynthesis. **Y.D.** and **E.S.S.** interpreted the data, and **Y.D.** wrote the manuscript with edits from **E.S.S.**

## COMPETING INTERESTS

The authors declare no competing interests related to this work.

## MATERIALS & CORRESPONDENCE

E.S.S. (sattely@stanford.edu) should be contacted for any materials or other correspondence.

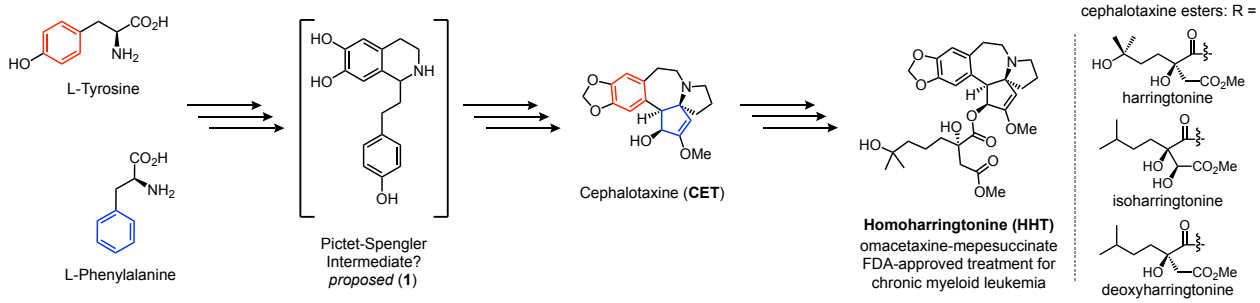


**Figure 1. Proposed biosynthetic pathway of CET, the core structure of HHT, and its esterified derivatives.** The proposed pathway for CET, the core structure of HHT, biosynthesis is based on radioisotope-labeling studies (shown in red and blue) and structural characterization of alkaloids from *Cephalotaxus* species. Over 20 distinct CET esters have been identified to date, four of which shown here exhibit notable biological activity. R denotes the variable ester side chain that can be attached to the CET core to form different CET esters (i.e. harringtonine, isoharringtonine, and deoxyharringtonine), whereas the HHT side chain is shown explicitly.

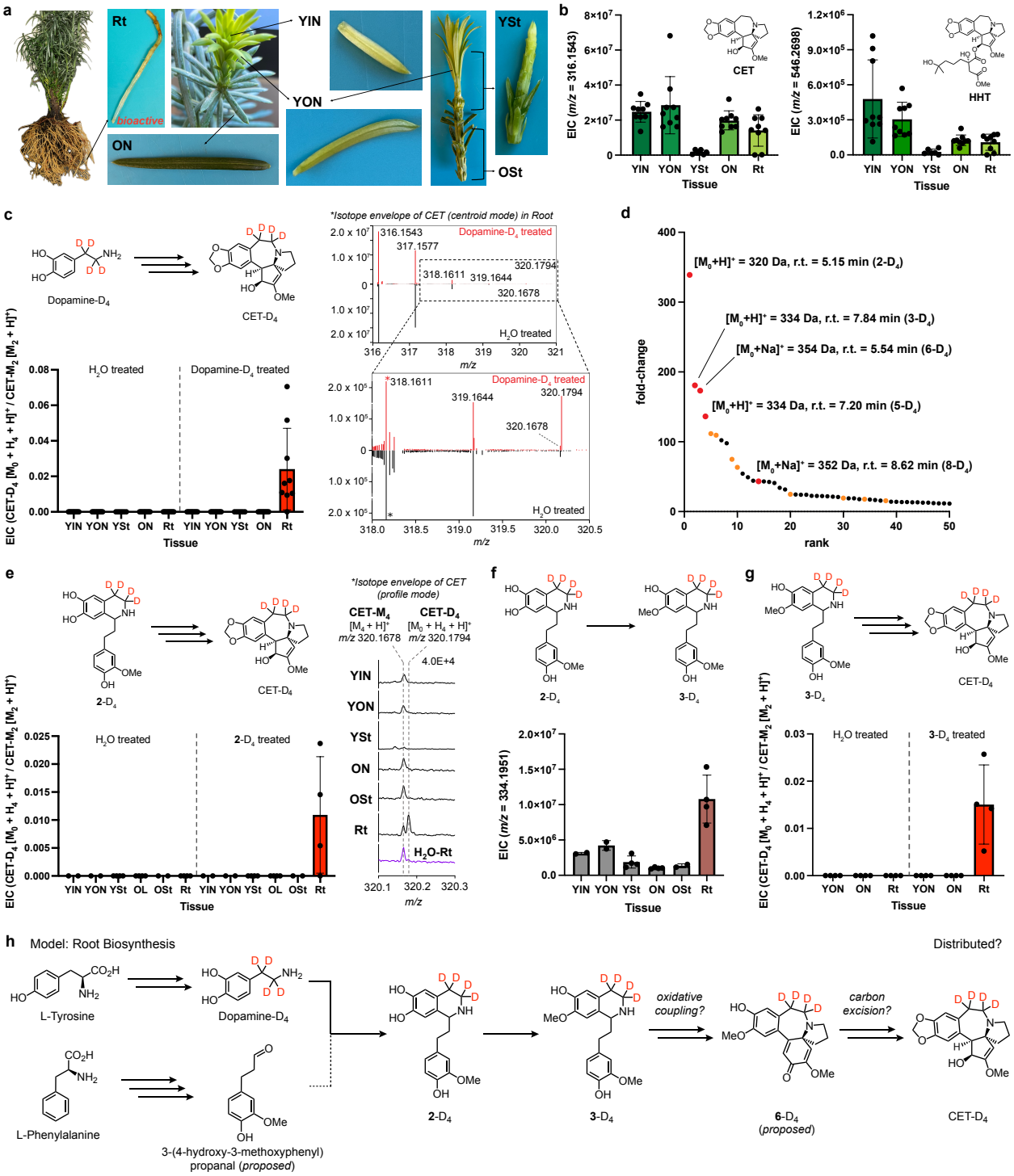


**Figure 2. Stable-isotope precursor feeding study reveals that root tips (up to length of approximately 5-8 cm) of actively growing plant are a site of active biosynthesis of cephalotaxine and that specific phenethylisoquinolines serve as intermediates in this process. (a)** Different tissues of *C. harringtonia* (young inner needles—YIN, young outer needles—YON, old needles—ON, young stem—YSt, old stem—OSt, and root tips—Rt) harvested during actively growing season of the plant (May or June) and dissected for paired feed-in experiments (metabolomics) and RNA-seq (transcriptomics). **(b)** Natural accumulation of CET ($[M + H]^+ = m/z$ 316.1543, r.t. = 2 min) and HHT ($[M + H]^+ = m/z$ 546.2698, r.t. = 10.8 min) throughout the native plant, *C. harringtonia* harvested in May 2022. **(c)** Relative isotope enrichment of CET-D4 in deuterated precursor dopamine-D4 feeding (right half of bar graph) compared to water treatment (left half of bar graph) in five different tissues

1098 indicates active biosynthesis of CET in the growing root tips (up to length of approximately 5-8 cm) of the native
1099 plant. On the right, isotope envelope of CET in centroid mode, comparing dopamine-$D_4$ treated Rt (red) vs $H_2O$
1100 treated Rt (black), is shown—with dopamine-$D_4$ treated Rt having an extra peak of *m/z* 320.1794 corresponding to
1101 CET-$D_4$ ($[M_0 + H_4 + H]^+$). **(d)** Untargeted metabolite analysis (XCMS) comparing dopamine-$D_4$ fed roots tips to
1102 water-fed root tips of *C. harringtonia* ($n = 9$ independent replicates for each experimental condition). The unique
1103 mass features ($P < 0.2$; fold change > 3.5; $200 < m/z < 600$) are ranked based on their increasing fold change in
1104 abundance between the two conditions, with top 50 shown. Features confirmed to be above signal to noise and
1105 represent true mass signatures corresponding to potential intermediates (with four deuteriums, resulting from
1106 incorporation of dopamine-D4) in CET biosynthesis are shown in red and their isotopologues and/or adducts in
1107 orange. r.t., retention time. While not shown here, CET-$D_4$ ranked 127$^{th}$ out of 148 unique features identified by
1108 XCMS with increasing fold change. **(e)** Relative isotope enrichment of CET-$D_4$ in **2**-$D_4$ feeding (right half of bar
1109 graph) compared to water treatment (left half of bar graph) in six different tissues indicates active biosynthesis of
1110 CET in the growing root tips (up to length of approximately 5-8 cm) of the native plant and **2**-$D_4$ as an intermediate
1111 in CET biosynthesis. On the right, isotope envelope of CET in **2**-$D_4$ fed tissues (YIN, YON, YSt, ON, OSt, and Rt)
1112 and in $H_2O$ fed Rt in profile mode, focusing on the fourth isotope peak, $M_4$ (M + 4), is shown. In the **2**-$D_4$ fed Rt
1113 sample, an additional fourth isotope peak appears at *m/z* 320.1794, corresponding to CET-$D_4$ ($[M_0 + H_4 + H]^+$) due
1114 to four deuterium incorporation, which is distinct from the natural carbon isotope peak at *m/z* 320.1678,
1115 corresponding to CET-$M_4$ ($[M_4 + H]^+$) observed in all different tissues fed with **2**-$D_4$ or water. **(f)** Observation of **3**-
1116 $D_4$ ($[M + H]^+$ = *m/z* 334.1951, r.t. = 7.8 min) in all six different tissues treated with **2**-$D_4$. O-methylation of **2**-$D_4$ to
1117 **3**-$D_4$ predominantly occurs in the actively growing root tips. **(g)** Relative isotope enrichment of CET-$D_4$ in **3**-$D_4$
1118 treatment (right half of bar graph) compared to water treatment (left half of bar graph) in three different tissues
1119 indicates active biosynthesis of CET in the growing root tips (up to length of approximately 5-8 cm) of the native
1120 plant and **3**-$D_4$ as an intermediate in CET biosynthesis. **(h)** Summary of updated proposed biosynthetic pathway for
1121 CET with stable-isotope precursor feeding experiments. Dotted line represents proposed aldehyde incorporation not
1122 yet supported by labeling studies. For all quantification, EIC of LC-MS was used. For CET-$D_4$ enrichment studies
1123 **(c, e, g)**, CET-$D_4$ was normalized by $M_2$ (M + 2) isotopologue to avoid detector saturation effects, since CET
1124 ionized well in LC-MS and was highly abundant in our measurement conditions. Experiments in **(b-d), (e-f),** and **(g)**
1125 were conducted in May 2022 ($n = 9$ biological replicates for each tissue type, except YSt, $n = 6$), in May 2023 ($n = 4$
1126 biological replicates for YSt, ON, and Rt, and $n = 2$ for YIN, YON, and OSt), and in June 2024 ($n = 4$ biological
1127 replicates for each tissue type) respectively. The values and error bars are mean and ± standard deviation (SD).
1128
1129
1130

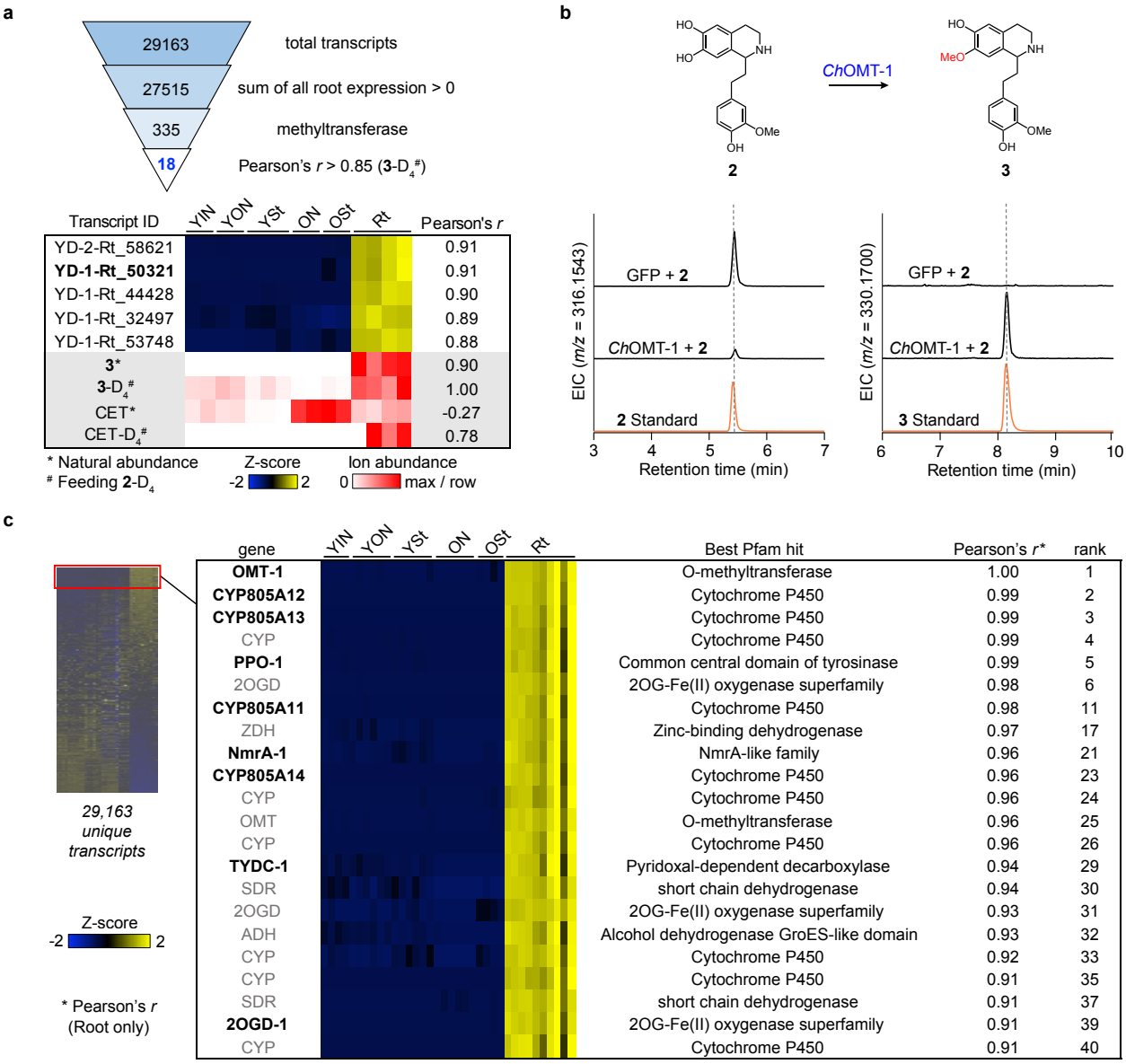


**Figure 3. Combined transcriptomics and metabolomics analysis identifies *Ch*OMT-1 as the biosynthetic gene and reveals co-expressed candidate genes involved in CET biosynthesis. (a)** The funnel plot shows the transcript selection process from 29,163 total transcripts to 18 candidate methyltransferases. The heatmap shows expression profiles (Z-score scaled) of the five (out of 18) tested methyltransferase-annotated transcripts in 15 samples of six different tissues of *C. harringtonia* from an independent experiment A conducted in May 2023, selected based on expression in root tips (site of active biosynthesis) and strong correlation with **3**-$D_4$ enrichment following **2**-$D_4$ feeding (Pearson's $r > 0.85$). Transcripts are ordered by decreasing correlation, with YD-1-Rt_50321 (in bold) identified as *Ch*OMT-1. Below, a metabolomic heatmap (red scale) shows LC-MS ion abundances of **3** and CET at natural isotope abundance (*) and their four-deuterated analogs (#) after **2**-$D_4$ feeding, measured in the same *C. harringtonia* tissues used for transcriptomic analysis (each tissue was divided for parallel profiling). Six different tissues (15 samples): 2 young inner needles (YIN), 2 young outer needles (YON), 3 young stems (YSt), 2 old needles (ON), 2 old stems (OSt), and 4 root tips (Rt). **(b)** Expression of *Ch*OMT-1 in *N. benthamiana* with co-infiltrated **2** leads to consumption of **2** (*m/z* 316.1543, r.t. of 5.4 min) and production of an O-methylated compound **3** (*m/z* 330.1700, r.t. of 8.1 min), as shown by the LC-MS chromatograms. This experiment was repeated more than three times, with similar results observed each time. Retention times of authentic standards (orange traces) are shown for comparison. Note: minimal retention time shifts (~0.2-0.3 min) are often observed in LC-MS runs conducted at different times. **(c)** RNA-seq analyses across various tissue types—YIN, YON, YSt, ON, OSt, and

Rt—combined with Pearson's correlation using *Ch*OMT-1 as the bait gene, identify a set of strongly co-expressing biosynthetic gene candidates from 29,163 unique transcripts. Initial Pearson correlation analysis across all tissues using *Ch*OMT-1 as a query gene identified 316 transcripts (r > 0.98). As many of these showed expression only in root tips, a second round of correlation analysis was conducted using Rt samples alone, yielding 41 top candidates (r > 0.90). Out of 41, genes of biosynthetically relevant enzyme families such as oxidases, reductases, O-methyltransferases, and pyridoxal phosphate (PLP)-dependent enzymes are shown here, and those involved in CET biosynthesis are highlighted in bold. Expression values within the heat map are $\log_2$-transformed values of each transcript calculated as Trimmed mean of M (TMM)-normalized counts per million (CPM) in Z-score scale. Pearson's *r* shown here are from the second round of correlation analysis done using only Rt samples. The whole heatmap is composed of 36 unique samples—YIN (4), YON (6), YSt (6), ON (6), OSt (4), and Rt (10)—harvested from the same plant but at two different times (one set, A, harvested in early May 2023 and the other set, B, two weeks after).

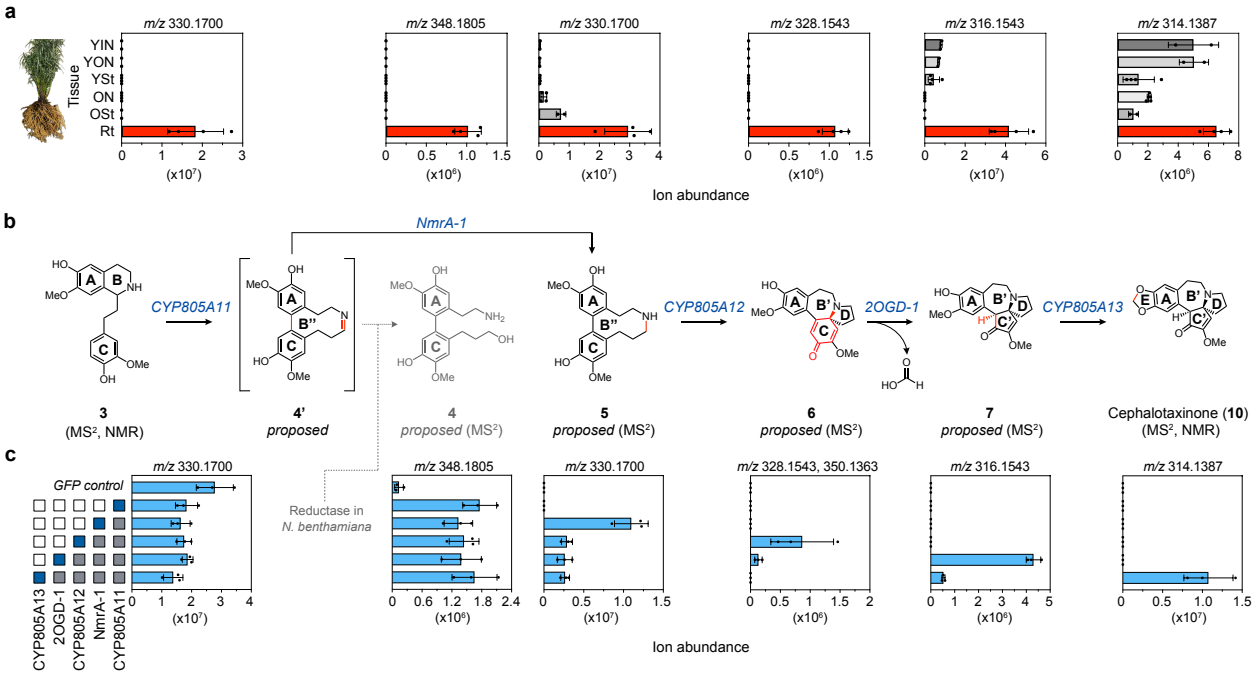


**Figure 4. Discovery of a pathway for CET alkaloid biosynthesis, from phenethylisoquinoline (3) to cephalotaxinone. (a)** Natural accumulation of CET biosynthetic intermediates in the native plant, *C. harringtonia*, harvested in May 2023. The data are reported as mean ± SD of the extracted ion abundance ($n$ = 4 biological replicates for YSt, ON, and Rt, and $n$ = 2 for YIN, YON, and OSt) for the exact ion mass $[M + H]^+$ corresponding to each compound. For quantification of cephalotaxinone, a 200-fold dilution was performed to the extracted samples to avoid saturation of the parent isotope peaks in LC-MS. Young inner needles (YIN), young outer needles (YON), Young stems (YSt), old needles (ON), old stems (OSt), and root tips (Rt). **(b)** Proposed biosynthetic pathway of CET reconstituted in *N. benthamiana* through transient co-expression of five identified biosynthetic genes from *C. harringtonia*, illustrating the stepwise conversion from compound **3** to cephalotaxinone (**10**). All the structures are supported by LC-MS/MS analyses, with the first and final intermediates (**3** and cephalotaxinone) further supported by authentic synthesized and purified standards, including NMR analyses. **(c)** Gray boxes to the left of the graphs indicate biosynthetic genes that are co-expressed in *N. benthamiana* leaves; blue box represents the final acting enzyme. For each intermediate, the data are reported as mean ± SD of the extracted ion abundance ($n$ = 3) for the exact ion mass $[M + H]^+$ (for **6**, both $[M + H]^+$ and $[M + Na]^+$) corresponding to each compound. While the overall biosynthetic pathway of CET is linear as shown, the final steps involving *Ch*CYP805A13 and *Ch*2OGD-1 may occur in bifurcated sequence (Extended Data Fig. 8).

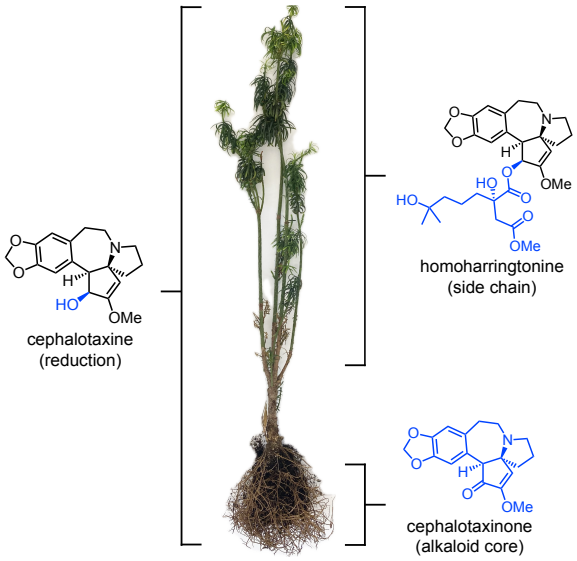


**Figure 5. Proposed model illustrating sites of active metabolism for whole plant coordination of *Cephalotaxus* alkaloid biosynthesis.** Proposed tissue specific metabolism is indicated in the parenthesis. Molecular components that are proposed to be actively produced, based on stable-isotope labeled precursor feeding and $D_2O$ labeling studies, are highlighted in blue.

1213 **REFERENCES**

1214


1215 1 Pérard-Viret, J., Quteishat, L., Alsalim, R., Royer, J. & Dumas, F. in *The Alkaloids: Chemistry*
1216 *and Biology* Vol. 78 (ed Hans-Joachim Knölker) 205-352 (Academic Press, 2017).
1217 2 Abdelkafi, H. & Nay, B. Natural products from *Cephalotaxus* sp.: chemical diversity and
1218 synthetic aspects. *Nat. Prod. Rep.* **29**, 845-869 (2012).
1219 3 Takano, I. et al. Ester-type cephalotaxus alkaloids from *Cephalotaxus harringtonia* var.
1220 *Drupacea*. *Phytochemistry* **44**, 735-738 (1997).
1221 4 Powell, R. G., Weisleder, D. & Smith, C. R., Jr. Antitumor alkaloids for *Cephalataxus*
1222 harringtonia: structure and activity. *J. Pharm. Sci.* **61**, 1227-1230 (1972).
1223 5 Powell, R. G., Weisleder, D., Smith, C. R. & Rohwedder, W. K. Structures of harringtonine,
1224 isoharringtonine, and homoharringtonine. *Tetrahedron Lett.* **11**, 815-818 (1970).
1225 6 Mikolajczak, K. L., Powell, R. G. & Smith, C. R. Deoxyharringtonine, a new antitumor alkaloid
1226 from *Cephalotaxus*: structure and synthetic studies. *Tetrahedron* **28**, 1995-2001 (1972).
1227 7 Zhou, J. Y., Chen, D. L., Shen, Z. S. & Koeffler, H. P. Effect of homoharringtonine on
1228 proliferation and differentiation of human leukemic cells in vitro. *Cancer Res.* **50**, 2031-2035
1229 (1990).
1230 8 Kantarjian, H. M., O'Brien, S. & Cortes, J. Homoharringtonine/omacetaxine mepesuccinate: the
1231 long and winding road to food and drug administration approval. *Clin. Lymphoma Myeloma Leuk.*
1232 **13**, 530-533 (2013).
1233 9 Lü, S. & Wang, J. Homoharringtonine and omacetaxine for myeloid hematological malignancies.
1234 *J. Hematol. Oncol.* **7**, 2 (2014).
1235 10 Chen, Y.-f. & Fu, L.-w. Mechanisms of acquired resistance to tyrosine kinase inhibitors. *Acta*
1236 *Pharm. Sin. B.* **1**, 197-207 (2011).
1237 11 Gürel, G., Blaha, G., Moore, P. B. & Steitz, T. A. U2504 determines the species specificity of the
1238 A-site cleft antibiotics: the structures of tiamulin, homoharringtonine, and bruceantin bound to the
1239 ribosome. *J. Mol. Biol.* **389**, 146-156 (2009).
1240 12 Huang, M. T. Harringtonine, an inhibitor of initiation of protein biosynthesis. *Mol. Pharmacol.*
1241 **11**, 511-519 (1975).
1242 13 Garreau de Loubresse, N. et al. Structural basis for the inhibition of the eukaryotic ribosome.
1243 *Nature* **513**, 517-522 (2014).
1244 14 Tujebajeva, R. M., Graifer, D. M., Karpova, G. G. & Ajtkhozhina, N. A. Alkaloid
1245 homoharringtonine inhibits polypeptide chain elongation on human ribosomes on the step of
1246 peptide bond formation. *FEBS Lett.* **257**, 254-256 (1989).
1247 15 Ingolia, N. T., Brar, G. A., Rouskin, S., McGeachy, A. M. & Weissman, J. S. The ribosome
1248 profiling strategy for monitoring translation in vivo by deep sequencing of ribosome-protected
1249 mRNA fragments. *Nat. Protoc.* **7**, 1534-1550 (2012).
1250 16 Delfel, N. E. Alkaloid distribution and catabolism in *Cephalotaxus harringtonia*. *Phytochemistry*
1251 **19**, 403-408 (1980).
1252 17 Powell, R. G. Structures of homoerythrina alkaloids from cephalotaxus harringtonia.
1253 *Phytochemistry* **11**, 1467-1472 (1972).
1254 18 Ju, X. & Beaudry, C. M. Total synthesis of (-)-cephalotaxine and (-)-homoharringtonine via furan
1255 oxidation-transannular Mannich cyclization. *Angew. Chem. Int. Ed.* **58**, 6752-6755 (2019).
1256 19 Robin, J.-P. et al. The first semi-synthesis of enantiopure homoharringtonine via
1257 anhydrohomoharringtonine from a preformed chiral acyl moiety. *Tetrahedron Lett.* **40**, 2931-
1258 2934 (1999).
1259 20 Hiranuma, S. & Hudlicky, T. Synthesis of homoharringtonine and its derivative by partial
1260 esterification of cephalotaxine. *Tetrahedron Lett.* **23**, 3431-3434 (1982).
1261 21 Isono, N. & Mori, M. Total synthesis of (-)-cephalotaxine. *J. Org. Chem.* **60**, 115-119 (1995).

1262 22 Li, W. D. & Wang, Y. Q. A novel and efficient total synthesis of cephalotaxine. *Org. Lett.* **5**,
1263 2931-2934 (2003).
1264 23 Yang, Y. L., D.; Katsuki, T. *Cephalotaxus harringtonii*. The IUCN Red List of Threatened
1265 Species 2013. e.T39589A2929537 (2013).
1266 24 *Drugs@FDA: FDA-Approved Drugs - Omacetaxine mepusuccinate (NDA 203585)*,
1267 <https://www.accessdata.fda.gov/scripts/cder/daf/index.cfm?event=overview.process&ApplNo=2
1268 03585> (2024).
1269 25 *Omacetaxine Injection*, <https://medlineplus.gov/druginfo/meds/a613012.html> (2024).
1270 26 Parry, R. J. & Schwab, J. M. Biosynthesis of *Cephalotaxus* alkaloids. I. Novel mode of tyrosine
1271 incorporation into cephalotaxine. *J. Am. Chem. Soc.* **97**, 2555-2557 (1975).
1272 27 Parry, R. J., Chang, M. N. T., Schwab, J. M. & Foxman, B. M. Biosynthesis of the *Cephalotaxus*
1273 alkaloids. Investigations of the early and late stages of cephalotaxine biosynthesis. *J. Am. Chem.*
1274 *Soc.* **102**, 1099-1111 (1980).
1275 28 Schwab, J. M., Chang, M. N. & Parry, R. J. Biosynthesis of *Cephalotaxus* alkaloids. 3. Specific
1276 incorporation of phenylalanine into cephalotaxine. *J. Am. Chem. Soc.* **99**, 2368-2370 (1977).
1277 29 Qiao, F. et al. Elucidation of the 1-phenethylisoquinoline pathway from an endemic conifer
1278 *Cephalotaxus hainanensis*. *Proc. Natl. Acad. Sci. USA* **120**, e2209339120 (2023).
1279 30 Nett, R. S., Lau, W. & Sattely, E. S. Discovery and engineering of colchicine alkaloid
1280 biosynthesis. *Nature* **584**, 148-153 (2020).
1281 31 Jacobowitz, J. R. & Weng, J.-K. Exploring uncharted territories of plant specialized metabolism
1282 in the postgenomic era. *Annu. Rev. Plant Biol.* **71**, 631-658 (2020).
1283 32 Mehta, N., Meng, Y., Zare, R., Kamenetsky-Goldstein, R. & Sattely, E. A developmental gradient
1284 reveals biosynthetic pathways to eukaryotic toxins in monocot geophytes. *Cell* **187**, 5620-5637.
1285 e5610 (2024).
1286 33 Lau, W. & Sattely, E. S. Six enzymes from mayapple that complete the biosynthetic pathway to
1287 the etoposide aglycone. *Science* **349**, 1224-1228 (2015).
1288 34 Caputi, L. et al. Missing enzymes in the biosynthesis of the anticancer drug vinblastine in
1289 Madagascar periwinkle. *Science* **360**, 1235-1239 (2018).
1290 35 Nett, R. S. et al. $D_2O$ labeling to measure active biosynthesis of natural products in medicinal
1291 plants. *AIChE J.* **64**, 4319-4330 (2018).
1292 36 Lau, W., Sattely, E., Smolke, C. D. & Spormann, A. M. *Pathway Discovery and Engineering of*
1293 *Pharmaceuticals from Medicinal Plants*, (2017).
1294 37 in *Evolution of the Arborescent Gymnosperms: Pattern, Process and Diversity: Southern*
1295 *Hemisphere Focus* Vol. 2 (ed Christopher N. Page) 338-351 (Cambridge University Press, 2024).
1296 38 Tomlinson, P. B. & Zacharias, E. H. Phyllotaxis, phenology and architecture in *Cephalotaxus*,
1297 *Torreya* and *Amentotaxus* (Coniferales). *Bot. J. Linn. Soc.* **135**, 215-228 (2001).
1298 39 Nett, R. S., Dho, Y., Low, Y.-Y. & Sattely, E. S. A metabolic regulon reveals early and late
1299 acting enzymes in neuroactive Lycopodium alkaloid biosynthesis. *Proc. Natl. Acad. Sci. USA*
1300 **118**, e2102949118 (2021).
1301 40 Conesa, A. et al. A survey of best practices for RNA-seq data analysis. *Genome Biol.* **17**, 13
1302 (2016).
1303 41 Morris, J. S. & Facchini, P. J. Molecular origins of functional diversity in benzylisoquinoline
1304 alkaloid methyltransferases. *Front. Plant Sci.* **10**, 1058 (2019).
1305 42 Sainsbury, F., Thuenemann, E. C. & Lomonossoff, G. P. pEAQ: versatile expression vectors for
1306 easy and quick transient expression of heterologous proteins in plants. *Plant Biotechnol. J.* **7**,
1307 682-693 (2009).
1308 43 Nguyen, T.-D. & Dang, T.-T. T. Cytochrome P450 enzymes as key drivers of alkaloid chemical
1309 diversification in plants. *Front. Plant Sci.* **12**, 682181 (2021).
1310 44 Kakizaki, T. et al. A 2-oxoglutarate-dependent dioxygenase mediates the biosynthesis of
1311 glucoraphasatin in radish. *Plant Physiol.* **173**, 1583-1593 (2017).

45 Kawai, Y., Ono, E. & Mizutani, M. Evolution and diversity of the 2–oxoglutarate-dependent dioxygenase superfamily in plants. *Plant J.* **78**, 328-343 (2014).
46 Hong, B. et al. Biosynthesis of strychnine. *Nature* **607**, 617-622 (2022).
47 Nett, R. S. et al. Plant carbonic anhydrase-like enzymes in neuroactive alkaloid biosynthesis. *Nature* **624**, 182-191 (2023).
48 Martinez, S. & Hausinger, R. P. Catalytic mechanisms of Fe(II)- and 2-oxoglutarate-dependent oxygenases. *J. Biol. Chem.* **290**, 20702-20711 (2015).
49 Podust, L. M. & Sherman, D. H. Diversity of P450 enzymes in the biosynthesis of natural products. *Nat. Prod. Rep.* **29**, 1251-1266 (2012).
50 Mizutani, M. & Ohta, D. Diversification of P450 genes during land plant evolution. *Annu. Rev. Plant Biol.* **61**, 291-315 (2010).
51 Kupchan, S. M., Dhingra, O. P. & Kim, C.-K. New biogenetic-type approach to *Cephalotaxus* alkaloids and the mechanism of Schelhammera-type homoerythrinadienone formation in vitro. *J. Org. Chem.* **43**, 4464-4468 (1978).
52 Marino, J. P. & Samanen, J. M. Biogenetic-type approach to homoerythrina alkaloids. *J. Org. Chem.* **41**, 179-180 (1976).
53 Meloni, M. et al. Structural and biochemical characterization of *Arabidopsis* alcohol dehydrogenases reveals distinct functional properties but similar redox sensitivity. *Plant J.* **118**, 1054-1070 (2024).
54 Zhang, Y. et al. Bioinformatic analysis of short-chain dehydrogenase/reductase proteins in plant peroxisomes. *Front. Plant Sci.* **14**, 1180647 (2023).
55 Stammers, D. K. et al. The structure of the negative transcriptional regulator NmrA reveals a structural superfamily which includes the short-chain dehydrogenase/reductases. *EMBO J.* **20**, 6619-6626 (2001).
56 Kotaka, M. et al. Structural analysis of the recognition of the negative regulator NmrA and DNA by the zinc finger from the GATA-type transcription factor AreA. *J. Mol. Biol.* **381**, 373-382 (2008).
57 Mao, T. et al. Genome-wide characterization of NmrA-like proteins and the regulatory function of soybean GmNmrA6 in response to salt and oxidative stresses. *Environ. Exp. Bot.* **213**, 105447 (2023).
58 Persson, B. et al. The SDR (short-chain dehydrogenase/reductase and related enzymes) nomenclature initiative. *Chem. Biol. Interact.* **178**, 94-98 (2009).
59 Min, T. et al. Crystal structures of pinoresinol-lariciresinol and phenylcoumaran benzylic ether reductases and their relationship to isoflavone reductases. *J. Biol. Chem.* **278**, 50714-50723 (2003).
60 Salter, M. M., Kobayashi, J., Shimizu, Y. & Kobayashi, S. Direct-type catalytic three-component Mannich reactions leading to an efficient synthesis of *α*,*β*-diamino acid derivatives. *Org. Lett.* **8**, 3533-3536 (2006).
61 Guengerich, F. P. & Yoshimoto, F. K. Formation and cleavage of C–C bonds by enzymatic oxidation–reduction reactions. *Chem. Rev.* **118**, 6573-6655 (2018).
62 Díaz Chávez, M. L., Rolf, M., Gesell, A. & Kutchan, T. M. Characterization of two methylenedioxy bridge-forming cytochrome P450-dependent enzymes of alkaloid formation in the Mexican prickly poppy *Argemone mexicana*. *Arch. Biochem. Biophys.* **507**, 186-193 (2011).
63 Luk, L. Y. P., Bunn, S., Liscombe, D. K., Facchini, P. J. & Tanner, M. E. Mechanistic studies on norcoclaurine synthase of benzylisoquinoline alkaloid biosynthesis: an enzymatic Pictet−Spengler reaction. *Biochemistry* **46**, 10153-10161 (2007).
64 He, Y. R. et al. Alkaloids from *Cephalotaxus lanceolata* and their cytotoxicities. *Chem. Biodivers.* **10**, 584-595 (2013).
65 Brönstrup, M. & Sasse, F. Natural products targeting the elongation phase of eukaryotic protein biosynthesis. *Nat. Prod. Rep.* **37**, 752-762 (2020).

66 Zhu, F., Zhou, Y.-K., Ji, Z.-L. & Chen, X.-R. The plant ribosome-inactivating proteins play important roles in defense against pathogens and insect pest attacks. *Front. Plant Sci.* **9**, 146 (2018).
67 Grela, P., Szajwaj, M., Horbowicz-Drożdżal, P. & Tchórzewski, M. How ricin damages the ribosome. *Toxins* **11** (2019).
68 Bolger, A. M., Lohse, M. & Usadel, B. Trimmomatic: a flexible trimmer for Illumina sequence data. *Bioinformatics* **30**, 2114-2120 (2014).
69 Haas, B. J. et al. De novo transcript sequence reconstruction from RNA-seq using the Trinity platform for reference generation and analysis. *Nat. Protoc.* **8**, 1494-1512 (2013).
70 Langmead, B. & Salzberg, S. L. Fast gapped-read alignment with Bowtie 2. *Nat. Methods* **9**, 357-359 (2012).
71 Simão, F. A., Waterhouse, R. M., Ioannidis, P., Kriventseva, E. V. & Zdobnov, E. M. BUSCO: assessing genome assembly and annotation completeness with single-copy orthologs. *Bioinformatics* **31**, 3210-3212 (2015).
72 Fu, L., Niu, B., Zhu, Z., Wu, S. & Li, W. CD-HIT: accelerated for clustering the next-generation sequencing data. *Bioinformatics* **28**, 3150-3152 (2012).
73 Finn, R. D. et al. The Pfam protein families database: towards a more sustainable future. *Nucleic Acids Res.* **44**, D279-D285 (2016).
74 Berardini, T. Z. et al. The Arabidopsis information resource: making and mining the "gold standard" annotated reference plant genome. *Genesis* **53**, 474-485 (2015).
75 Xiong, X. et al. The Taxus genome provides insights into paclitaxel biosynthesis. *Nat. Plants* **7**, 1026-1036 (2021).
76 Bray, N. L., Pimentel, H., Melsted, P. & Pachter, L. Near-optimal probabilistic RNA-seq quantification. *Nat. Biotechnol.* **34**, 525-527 (2016).
77 Nett, R. S. & Sattely, E. S. Total biosynthesis of the tubulin-binding alkaloid colchicine. *J. Am. Chem. Soc.* **143**, 19454-19465 (2021).
78 Pompon, D., Louerat, B., Bronine, A. & Urban, P. in *Methods in Enzymology* Vol. 272 (eds Eric F. Johnson & Michael R. Waterman) 51-64 (Academic Press, 1996).
79 Urban, P., Mignotte, C., Kazmaier, M., Delorme, F. & Pompon, D. Cloning, yeast expression, and characterization of the coupling of two distantly related *Arabidopsis thaliana* NADPH-cytochrome P450 reductases with P450 CYP73A5. *J. Biol. Chem.* **272**, 19176-19186 (1997).
80 Recipe: complete minimal (CM) or synthetic complete (SC) and drop-out media. *Cold Spring Harb. Protoc.* https://doi.org/10.1101/pdb.rec8190 (2006).
81 Recipe: dropout mix. *Cold Spring Harb. Protoc.* https://doi.org/10.1101/pdb.rec8585 (2006).
82 Smith, C. A., Want, E. J., O'Maille, G., Abagyan, R. & Siuzdak, G. XCMS: processing mass spectrometry data for metabolite profiling using nonlinear peak alignment, matching, and identification. *Anal. Chem.* **78**, 779-787 (2006).
83 Pesnot, T., Gershater, M. C., Ward, J. M. & Hailes, H. C. Phosphate mediated biomimetic synthesis of tetrahydroisoquinoline alkaloids. *Chem. Commun.* **47**, 3242-3244 (2011).
84 Yamauchi, Y., Hasegawa, A., Taninaka, A., Mizutani, M. & Sugimoto, Y. NADPH-dependent reductases involved in the detoxification of reactive carbonyls in plants. *J. Biol. Chem.* **286**, 6999-7009 (2011).
85 Choi, H. W. et al. A role for a menthone reductase in resistance against microbial pathogens in plants. *Plant Physiol.* **148**, 383-401 (2008).
86 Mulichak, A. M., Theisen, M. J., Essigmann, B., Benning, C. & Garavito, R. M. Crystal structure of SQD1, an enzyme involved in the biosynthesis of the plant sulfolipid headgroup donor UDP-sulfoquinovose. *Proc. Natl. Acad. Sci. USA* **96**, 13097-13102 (1999).
87 Katoh, K., Misawa, K., Kuma, K. i. & Miyata, T. MAFFT: a novel method for rapid multiple sequence alignment based on fast Fourier transform. *Nucleic Acids Res.* **30**, 3059-3066 (2002).
88 Price, M. N., Dehal, P. S. & Arkin, A. P. FastTree 2–approximately maximum-likelihood trees for large alignments. *PLoS One* **5**, e9490 (2010).

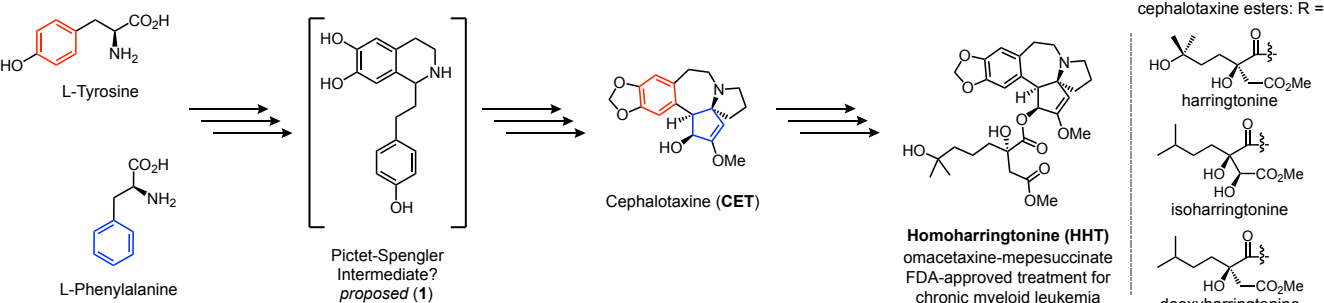
L-Tyrosine
L-Phenylalanine
Pictet-Spengler
Intermediate?
*proposed* (**1**)
Cephalotaxine (**CET**)
**Homoharringtonine (HHT)**
omacetaxine-mepesuccinate
FDA-approved treatment for
chronic myeloid leukemia
cephalotaxine esters: R =
harringtonine
isoharringtonine
deoxyharringtonine

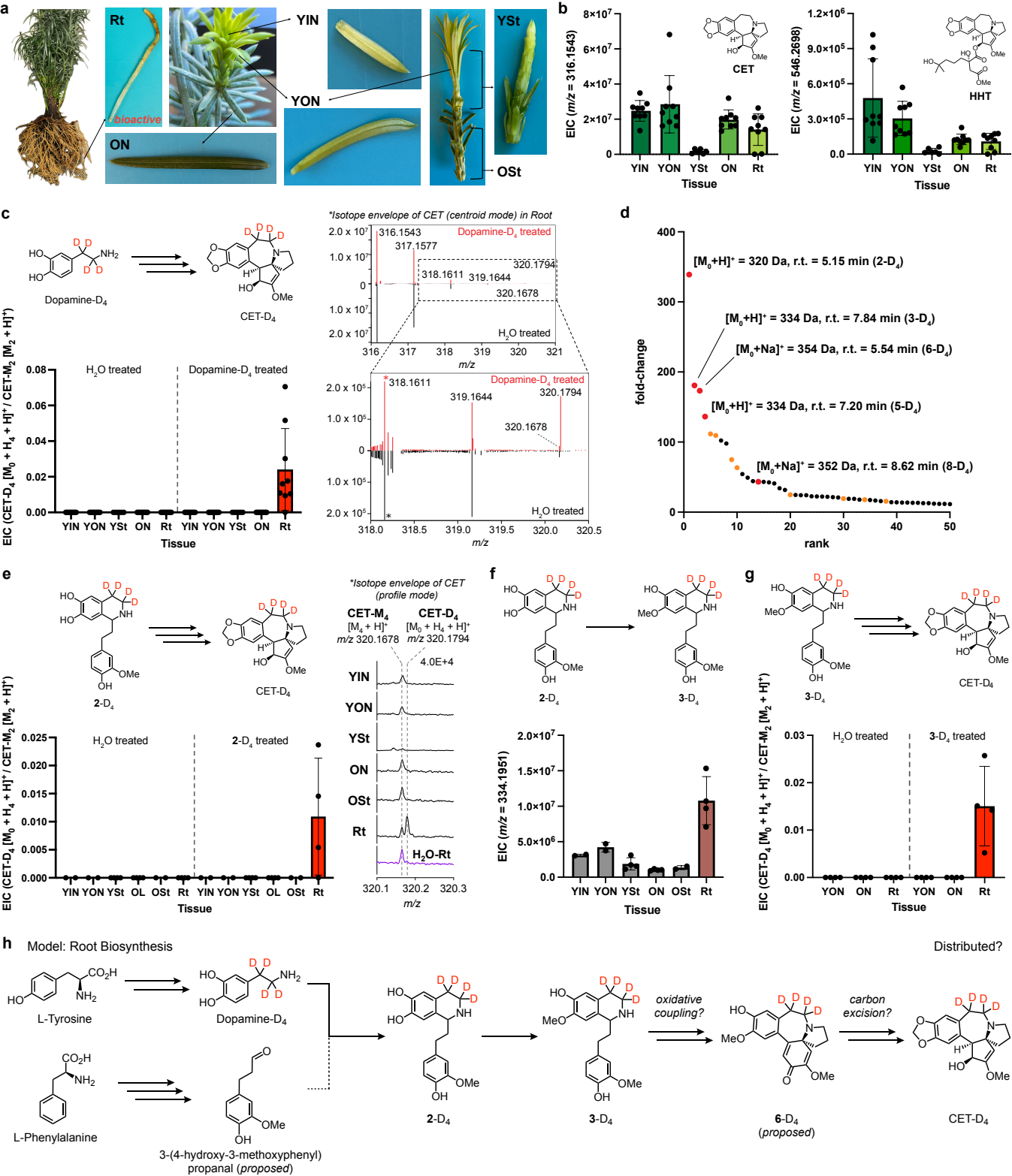
a
Rt
bioactive
YIN
YON
ON
YSt
OSt
b
EIC (m/z = 316.1543)
CET
EIC (m/z = 546.2698)
HHT
YIN YON YSt ON Rt
Tissue
c
Dopamine-D4
CET-D4
H2O treated
Dopamine-D4 treated
EIC (CET-D4 [M0 + H4 + H]+ / CET-M2 [M2 + H]+)
YIN YON YSt ON Rt YIN YON YSt ON Rt
Tissue
*Isotope envelope of CET (centroid mode) in Root
316.1543
317.1577
318.1611
319.1644
320.1794
320.1678
m/z
d
[M0+H]+ = 320 Da, r.t. = 5.15 min (2-D4)
[M0+H]+ = 334 Da, r.t. = 7.84 min (3-D4)
[M0+Na]+ = 354 Da, r.t. = 5.54 min (6-D4)
[M0+H]+ = 334 Da, r.t. = 7.20 min (5-D4)
[M0+Na]+ = 352 Da, r.t. = 8.62 min (8-D4)
fold-change
rank
e
2-D4
CET-D4
2-D4 treated
EIC (CET-D4 [M0 + H4 + H]+ / CET-M2 [M2 + H]+)
YIN YON YSt OL OSt Rt YIN YON YSt OL OSt Rt
Tissue
*Isotope envelope of CET (profile mode)
CET-M4 [M4 + H]+ m/z 320.1678
CET-D4 [M0 + H4 + H]+ m/z 320.1794
4.0E+4
YIN
YON
YSt
ON
OSt
Rt
H2O-Rt
m/z
f
2-D4
3-D4
EIC (m/z = 334.1951)
YIN YON YSt ON OSt Rt
Tissue
g
3-D4
CET-D4
3-D4 treated
EIC (CET-D4 [M0 + H4 + H]+ / CET-M2 [M2 + H]+)
YON ON Rt YON ON Rt
Tissue
h
Model: Root Biosynthesis
Distributed?
L-Tyrosine
Dopamine-D4
L-Phenylalanine
3-(4-hydroxy-3-methoxyphenyl) propanal (proposed)
2-D4
3-D4
oxidative coupling?
6-D4 (proposed)
carbon excision?
CET-D4

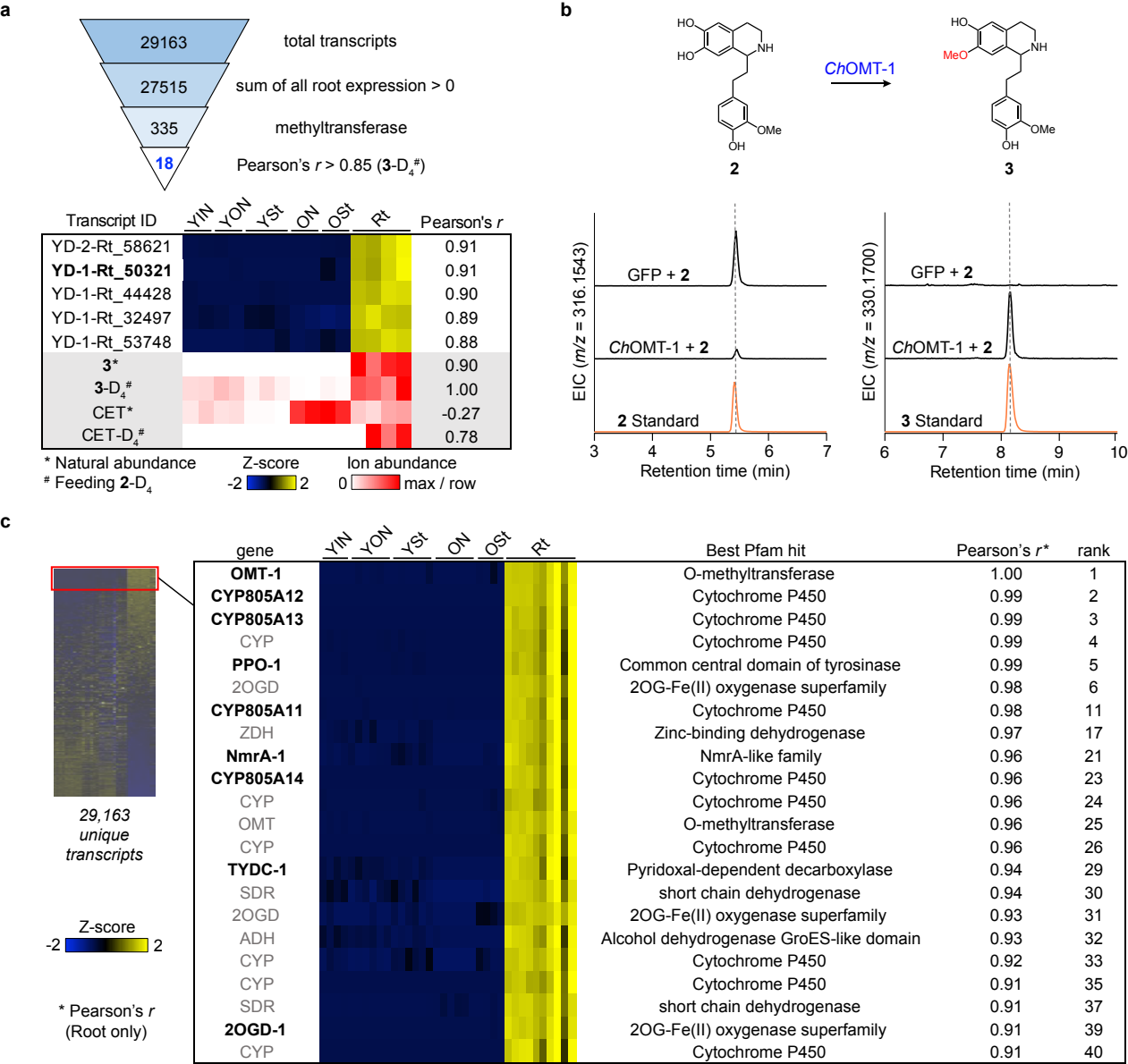
a
29163
total transcripts
27515
sum of all root expression > 0
335
methyltransferase
18
Pearson's r > 0.85 (3-D4#)
Transcript ID
YIN
YON
YSt
ON
OSt
Rt
Pearson's r
YD-2-Rt_58621 0.91
YD-1-Rt_50321 0.91
YD-1-Rt_44428 0.90
YD-1-Rt_32497 0.89
YD-1-Rt_53748 0.88
3* 0.90
3-D4# 1.00
CET* -0.27
CET-D4# 0.78
* Natural abundance
# Feeding 2-D4
Z-score
-2 2
Ion abundance
0 max / row
b
HO
HO
NH
OMe
OH
2
ChOMT-1
HO
MeO
NH
OMe
OH
3
EIC (m/z = 316.1543)
GFP + 2
ChOMT-1 + 2
2 Standard
3 4 5 6 7
Retention time (min)
EIC (m/z = 330.1700)
GFP + 2
ChOMT-1 + 2
3 Standard
6 7 8 9 10
Retention time (min)
c
29,163 unique transcripts
Z-score
-2 2
* Pearson's r (Root only)
gene
YIN
YON
YSt
ON
OSt
Rt
Best Pfam hit
Pearson's r*
rank
OMT-1 O-methyltransferase 1.00 1
CYP805A12 Cytochrome P450 0.99 2
CYP805A13 Cytochrome P450 0.99 3
CYP Cytochrome P450 0.99 4
PPO-1 Common central domain of tyrosinase 0.99 5
2OGD 2OG-Fe(II) oxygenase superfamily 0.98 6
CYP805A11 Cytochrome P450 0.98 11
ZDH Zinc-binding dehydrogenase 0.97 17
NmrA-1 NmrA-like family 0.96 21
CYP805A14 Cytochrome P450 0.96 23
CYP Cytochrome P450 0.96 24
OMT O-methyltransferase 0.96 25
CYP Cytochrome P450 0.96 26
TYDC-1 Pyridoxal-dependent decarboxylase 0.94 29
SDR short chain dehydrogenase 0.94 30
2OGD 2OG-Fe(II) oxygenase superfamily 0.93 31
ADH Alcohol dehydrogenase GroES-like domain 0.93 32
CYP Cytochrome P450 0.92 33
CYP Cytochrome P450 0.91 35
SDR short chain dehydrogenase 0.91 37
2OGD-1 2OG-Fe(II) oxygenase superfamily 0.91 39
CYP Cytochrome P450 0.91 40

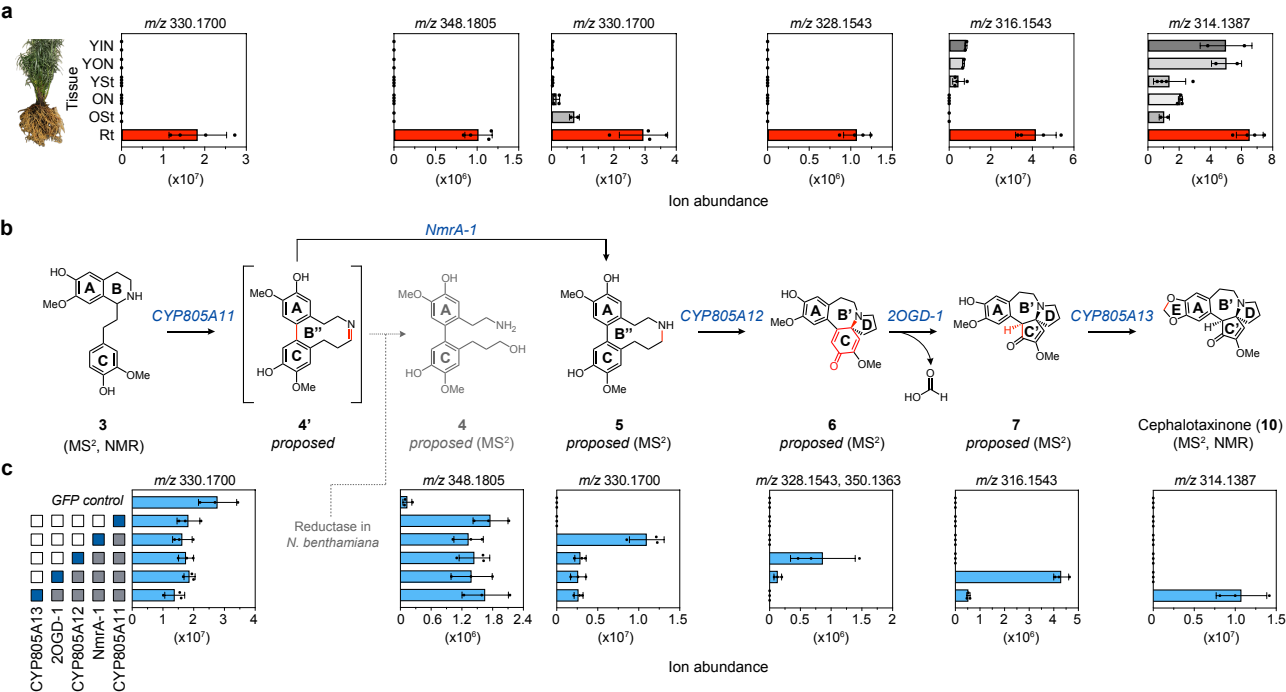
a
m/z 330.1700
m/z 348.1805
m/z 330.1700
m/z 328.1543
m/z 316.1543
m/z 314.1387
Tissue
YIN
YON
YSt
ON
OSt
Rt
(x10^7)
(x10^6)
Ion abundance
b
NmrA-1
CYP805A11
CYP805A12
2OGD-1
CYP805A13
3
(MS², NMR)
4'
proposed
4
proposed (MS²)
5
proposed (MS²)
6
proposed (MS²)
7
proposed (MS²)
Cephalotaxinone (10)
(MS², NMR)
c
GFP control
CYP805A13
2OGD-1
CYP805A12
NmrA-1
CYP805A11
Reductase in
N. benthamiana
m/z 330.1700
m/z 348.1805
m/z 330.1700
m/z 328.1543, 350.1363
m/z 316.1543
m/z 314.1387
(x10^7)
(x10^6)
Ion abundance

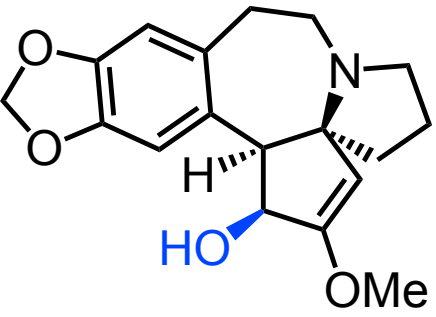


cephalotaxine
(reduction)

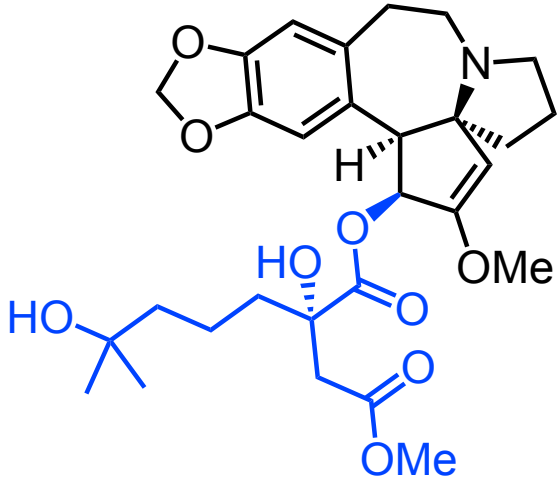


homoharringtonine
(side chain)

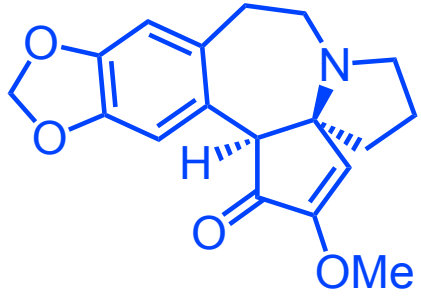


cephalotaxinone
(alkaloid core)